THE LOCALIZATION AND BEHAVIOR OF FLUORESCENTLY TAGGED MAGNETIC NANOPARTICLES IN BIOLOGICAL SYSTEMS

by

MARY KATHRYN SEWELL

A THESIS

Submitted in partial fulfillment of the requirements
for the degree of Master of Science in the Department
of Chemical and Biological Engineering
in the Graduate School of
The University of Alabama

TUSCALOOSA, ALABAMA

2009

ABSTRACT

A novel combination cancer therapy platform incorporating chemotherapy and hyperthermia is proposed. Magnetic nanoparticles are included as a way to achieve the hyperthermia treatment, as well as for use as a platform for targeting, imaging, or other therapeutic moieties. Cobalt ferrite ($CoFe_2O_4$) magnetic nanoparticles (MNPs) were synthesized and tagged with the fluorescent dye rhodamine for tracking in biological systems. The MNP solutions were characterized to determine average diameters of the nanoparticles. Results indicate that sample age, solvent, and concentration can affect the diameters of MNP agglomerates as measured by dynamic light scattering. Older and more concentrated samples, which also tend to be less stable, showed larger MNP sizes than newer and less concentrated samples. Rhodamine-tagged MNPs showed smaller diameters than untagged MNPs at the same concentrations. For MNP in HeLa cell localization studies, the rhodamine-tagged MNPs showed uptake and localization in the cytoplasm of the cells. Partition coefficients, or the ratios of MNP concentrations inside the cells to the extracellular concentration, were shown to increase during the first 6 h of incubation time, with values reaching as high as 3.805, indicating favorable uptake of the MNPs. After 24 h, a smaller ratio of internalized MNPs was seen due to cytotoxic properties of the high concentration of MNPs used in those experiments. Toxicity studies showed that at concentrations below approximately 0.025 mg/mL, both rhodamine-tagged and untagged $CoFe_2O_4$ MNPs have little effect on cell viability. MNP localization and toxicity studies were also carried out on a model organism, *C. elegans* worms, with an indication that rhodamine-tagged $CoFe_2O_4$ MNPs were non-toxic to worms over a period of 12 days.

Localization of the MNPs within the worms was inconclusive due to indistinguishable autofluorescence of the *C. elegans* and the rhodamine fluorescence of tagged MNPs. Further work is needed to characterize the $CoFe_2O_4$ MNPs for use in the cancer treatment platform.

DEDICATION

This thesis is dedicated to all of my friends, family members, and professors who helped me through my research project. They have inspired me to achieve many successes, including this thesis. Special thanks is deserved by those who stood beside me, motivated me, and helped me with the writing and editing processes, especially the other graduate students in the Department of Chemical and Biological Engineering.

ACKNOWLEDGEMENTS

I would like to take this opportunity to thank everyone involved with my research project and my lab group. Most importantly, I wish to thank Dr. Christopher Brazel, who has been my advisor for three years. He has been a great source of inspiration, motivation and wisdom through both of my projects. I would also like to acknowledge my thesis committee members including Dr. Yuping Bao, Dr. Carol Duffy, and Dr. David Nikles. Dr. Steven Ritchie, the Director of Graduate Studies in the Department of Chemical and Biological Engineering, also deserves thanks for helping me through the program, given my unique and interesting set of circumstances. For helping me with my HeLa cell studies, I wish to thank Dr. Maaike Everts in Gene Therapy at the University of Alabama at Birmingham and all of her students. I also wish to thank The University of Alabama Graduate School and Department of Chemical and Biological Engineering, for providing me funding while I completed this project. I also need to thank Dr. Kim Lackey for assisting me with the use of the fluorescence and confocal microscopes at The University of Alabama.

Finally, I want to thank the members of the former and current Magnetic Biomaterials Research Group, especially Dr. Dong Hyun Kim, Dr. Indu Ankareddi, John Melnyczuk, Lauren Blue, Kyle Fugit, and Amy Frees.

CONTENTS

LIST OF TABLES

LIST OF FIGURES

Chapter 1

INTRODUCTION

The application of nanotechnology to the medical field represents a novel approach to how to treat diseases. The emerging discipline of nanomedicine, where an aspect of the treatment platform is on the nanoscale, proposes direct interaction between the treatment platform and the biological system of choice. Nanoparticles are capable of acting as a new treatment method because they can interact with individual cells within a body, as well as viruses or bacteria that cause a wide variety of diseases. The use of nanoparticles in medicine has been proposed in numerous areas including imaging, cell tracking, biosensors, bioseparations, targeted drug delivery, tissue engineering, magnetic transfection, and cancer treatment [1, 2, 3]. Within these broad topics, further investigation has led to the application of nanomedicine to treat a variety of systems including the gastrointestinal tract, musculoskeletal system, nervous system, and cardiovascular system [4]. This project focuses on the potential for magnetic nanoparticle inclusion in a novel combination cancer treatment platform.

As of 2007, the National Cancer Institute reported that over 11 million Americans had been diagnosed with cancer. An additional 1.5 million cases were diagnosed over the course of the next year, and over 500,000 people died from cancer related causes [5]. Current treatments for many types of cancer are inefficient and costly, both financially and personally. The common treatments, such as radiation, surgery, and chemotherapy, carry risks and disadvantages for every patient. Negative side effects associated with current treatment methodology can lower

the patient's quality of life. To better help the millions of afflicted individuals, novel treatments are required; these platforms will combine current methodologies with better targeting and control of delivery. Overall, this will improve treatment efficacy, decrease the risk of negative side effects, and lead to better quality of care for the patient.

Creating the "perfect" cancer treatment is difficult because cancer is not a single disease, but rather a variety of diseases related by the underlying cause: the uncontrollable growth of cells [6]. This increased difficulty is reflected in cancer mortality statistics. Since 1950, the mortality rate of cancer has not declined [7]. As Figure 1.1 shows, among the leading causes of death in the United States, cancer is the only one that has not shown a decrease in mortality. This disease affects people from every ethnic, age, and socio-economic background. Because of the severity and range of the condition, novel treatments are needed to improve quality of care for afflicted patients.

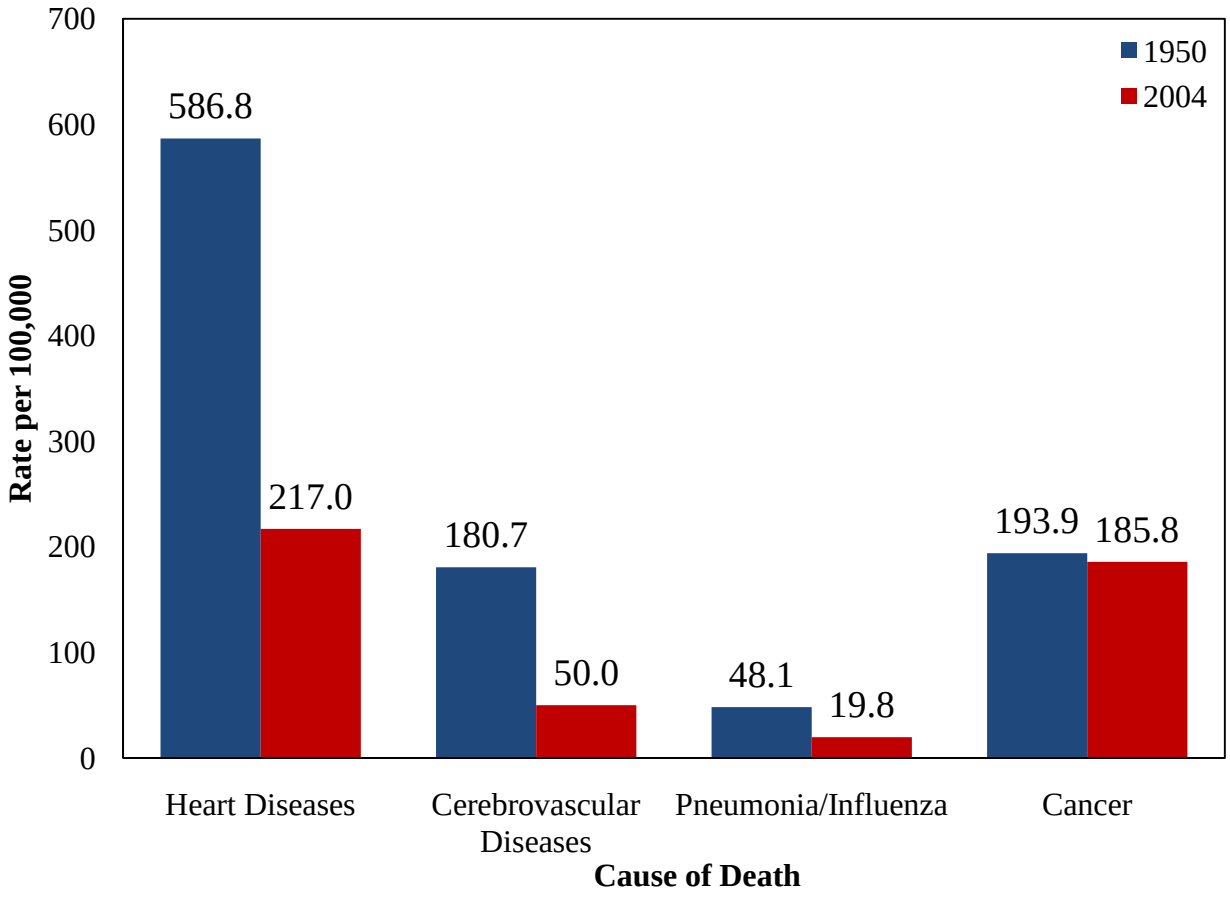

Figure 1.1 Mortality Rates of Leading Causes of Death in the United States from 1950 to 2004. Age-adjusted to 2000 US Standard Population. Sources: 1950 Mortality Data - CDC/NCHS, NVSS, Mortality Revised [7].

Nanotechnology offers a new approach to treating cancer. Nanoparticles can be created and functionalized specifically for cancer treatment platforms. The National Cancer Institute has created an outline of what a nanotech-cancer treatment should contain, as shown in Figure 1.2 [8]. The nanoplatform must be able to perform imaging and diagnostics, contain a targeting moiety, contain a therapeutic moiety, and be able to report the success of the treatment once triggered. This combination will allow for both the detection and treatment of tumors. After treatment, the nanoplatform will then be able to report to the doctors about the success of the treatment. Because of the targeting moiety, the therapeutic agent will be localized to only the cancerous cells. This should increase efficacy of the treatment, while eliminating some negative side effects.

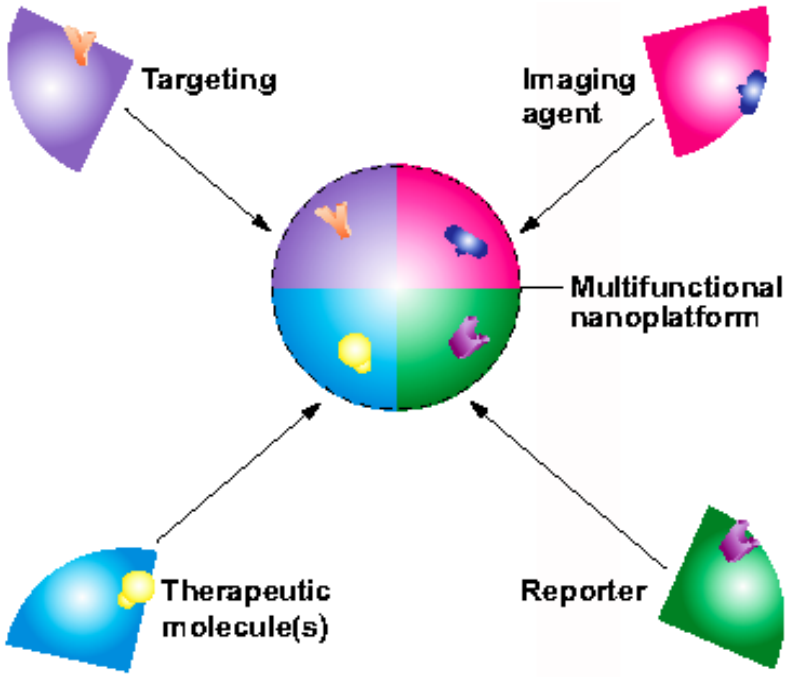

Figure 1.2 Graphical Representation of Multifunctional Nanoplatform for Cancer Treatment. Based on Initiative of the NCI Alliance for Nanotechnology in Cancer [8].

The potential advantages of a nanoparticle treatment platform stem from the interesting and unique characteristics of the nanoparticles themselves. Because of their size, nanoparticles are capable of acting on the cellular level as vectors for drug delivery or gene therapy. Nanoparticles' unique physical properties allow the functionalization and surface modification that provide a novel method for targeted therapy. However, these approaches are largely untested and not well characterized because of their novelty. Before medical nanoparticles can be widely applied, their biological behaviors must be understood. The behaviors of interest include how nanoparticles can attach and adsorb onto cell membranes, as well as how the particles are internalized and localized within the cell. The localization of nanoparticles at the cellular, tissue, and whole organism levels will determine how the treatment platforms are designed. Knowing how nanoparticles are metabolized and removed from the body is also an important issue. Understanding these properties is a fundamental step in the evolution of nanoplatforms for cancer treatment.

The Magnetic Biomaterials Research Group at The University of Alabama is dedicated to developing a novel combination cancer treatment platform that will improve how cancer patients are treated. The proposed platform combines chemotherapy and hyperthermia by utilizing a thermally responsive hydrogel embedded with therapeutic agent and magnetic nanoparticles. When subjected to an external AC magnetic field, the nanoparticles will heat. The heat triggers the thermal response of the hydrogel, controlling the release of an anti-cancer agent. The focus of this project is to study the behavior of the proposed magnetic nanoparticles in biological systems.

Chapter 2

BACKGROUND

The potential application of magnetic nanoparticles for cancer therapy has received growing interest in the past few years. Previous work has been done to test the viability of such platforms. The following section details current cancer treatment methodologies, along with disadvantages of each type of treatment. A more detailed discussion is included on hyperthermia therapy, as magnetic nanoparticles can be used to deliver localized heating. Also, the typical applications of magnetic nanoparticles in medicine are discussed, including both therapeutic and diagnostic uses. Finally, the section includes discussion of interactions between cells and nanoparticles. Previous projects showing the toxicological properties, as well as localization and uptake mechanisms, are highlighted.

2.1 Current Cancer Treatments

Current cancer treatments include surgery, chemotherapy, and radiation [9]. Often, a combination of these is utilized to increase the effectiveness of the treatment. However, each of the methods comes with numerous side effects that can decrease the quality of life for patients. When a tumor is removed surgically, the surgeon has no way of knowing if he or she has removed all of the cancerous cells. Even if the bulk of the tumor has been excised, the doctor cannot see individual cancer cells to know if they have all been removed. In other cases, such as specific types of brain tumors, surgery may not even be an option.

Chemotherapy involves a massive dose of an anti-cancer agent into a patient's body. Because the levels of the drug are so high, and the drug is toxic to cells, chemotherapy often causes "collateral damage" in the body. While the anti-cancer drug may be specific to cancerous cells, healthy cells may also be damaged or killed. This leads to common side effects such as nausea, hair-loss, and fatigue. In radiation therapy, ionizing radiation is targeted to a tumor. Unfortunately, this therapy can also harm other systems; an example of this damage is the weakening of the skeletal system. The idea of combination of multiple therapies to increase treatment efficacy has been around for over three decades [10]. A study done by Herskovic showed that combination of chemotherapy and radiation treatment for patients with esophageal cancer increased the median 12-month survival rate from 33% to 50% over patients treated with radiation alone [11]. Unfortunately, the risk of "severe" side effects increased from 25% for the single therapy group to 44% for the combination treatment group.

A growing area of interest is hyperthermia therapy [12, 13, 14]. Hyperthermia is a treatment in which a patient is subjected to heating to temperatures ranging from 42-45^{o}C [12, 13, 14]. At hyperthermic conditions, cancerous cells are preferentially killed rather than healthy cells [12, 15]. This is due to the cancer cells incomplete vascular network, which prevents the cells from dissipating the heat as effectively as healthy cells [12, 15]. The heating may be whole body, regional, or localized to an affected region [12, 16]. Whole body hyperthermia does not localize the heating effects, which can lead to negative side effects in unaffected areas of a patient's body [12, 16, 17]. However, the novel approach is magnetic fluid hyperthermia (MFH) in which magnetic nanoparticles (MNPs) are used. In a study by Jordan, the growth rate of tumors was controlled using MFH where dextran-coated magnetite nanoparticles were injected

into the tumors of mice [18]. After 60 days, 44% of the MFH-treated mice showed little to no additional tumor growth.

2.2 Applications of Magnetic Nanoparticles in Medicine

The rise of nanotechnology in the last twenty years or so has led to the creation of the field of nanomedicine. This encompasses numerous subdivisions in a variety of specialties and includes regenerative medicine, as well as combination treatment platforms. Magnetic nanoparticles are being proposed as the next generation of therapeutic agents in everything from cancer to atherosclerosis [1, 2, 12, 18, 19, 20, 21]. In addition to treatment methodologies, nanoparticles are now being utilized for enhanced diagnostics and imaging [1, 4]. Because MNPs can be used to label specific cells in the central nervous system, they may improve imaging of spinal cord injuries, multiple sclerosis, brain tumors, and stroke damage [20]. Other current research projects are using nanotechnology to create new targeting methods [1, 22]. One such method includes using externally-applied magnetic fields to localize the MNPs [14]. Other approaches incorporate antigens or ligands for use with cell membrane receptors [2, 15, 23]. The projects represent the different aspects of the NCI initiative for a nanotech cancer treatment. Additional applications of magnetic nanoparticles include tissue engineering, biosensors, and bioseparations [1, 2]. In tissue repair, iron oxide nanoparticles are proposed as novel targeting and activating agents for the process of welding damaged tissues back together [2, 15, 24, 25]. For bioseparations and biosensing, magnetic nanoparticles functionalized with antibodies can be used to screen out infective agents from blood or to detect the presence of specific proteins [26, 27].

2.2.1 Magnetic Nanoparticles as Therapeutic Agents

As therapeutic agents, nanoparticles will have the ability to interact on the cellular level with the diseases they are designed to fight [1, 2, 21, 23]. Because of their size and unique properties, they can travel to and interact with parts of the body that are inaccessible to current medical technology. For example, nanoparticles have the potential to pass through the blood-brain barrier, allowing them to target inoperable brain tumors [2, 28]. Magnetic nanoparticles have been proposed in many of these systems because of their unique physical properties. However, because of their novelty in the medical field, their toxicity and biocompatibility are not well understood [29]. Before implementation in treatment platforms, the behavior of magnetic nanoparticles in the human body must be fully investigated. This includes how nanoparticles are taken up by cells, localization methods and patterns, bioaccumulation, and excretion from the body.

Magnetic nanoparticles are being investigated as a way of achieving localized and externally triggered hyperthermia for cancer patients [18, 30]. The addition of polymer coatings, such as dextran, as surface modifications on the MNPs increases circulation time and improved targeting for hyperthermia therapy [1, 2, 31]. Two of the most common materials investigated for magnetic hyperthermia are magnetite and maghemite, because of their biocompatibility as well as desirable magnetic properties [32]. The specific absorption ratios (SARs) of these materials are high enough to facilitate rapid heating to hyperthermic temperatures. Other materials such as cobalt ferrite and manganese ferrite are being investigated as agents for hyperthermia and enhanced contrast for magnetic resonance imaging (MRI) [19, 32]. These particles show excellent heating rates when exposed to AC magnetic fields and are considered biocompatible because of a cobalt ferrite layer that surrounds the particles [19, 33].

The heating capabilities of magnetic nanoparticles are determined by composition and size [34]. While the efficient heating of MNPs is desired, there must be limitations in place to prevent any damage to the healthy tissues of the patient. Brezovich reports that there are limiting values for magnetic field magnitudes and frequencies in hyperthermic applications [35]. However, intense fields might be viable if used in multiple, short durations rather than a single long duration.

2.2.2 Magnetic Nanoparticles for Imaging and Diagnostics

One of the most common applications of nanoparticles, magnetic or nonmagnetic, is in the field of imaging and diagnostics. MRI has been an effective method for visualizing tumors and other diseases for many years [36, 37]. Magnetic resonance imaging works by measuring the variations in proton density and relaxation times of protons in water [36, 37]. The imposed magnetic field from the imaging device causes alignment of these protons, before the introduction of a radio frequency electromagnetic, which excites the protons. When the field is turned off and the protons relax, the relaxation times differ for different types of tissues [36, 37]. The inclusion of agents that increase the magnetic signal thus enhance the contrast of images obtained by MRI [36, 37]. Current MRI technology relies on gadolinium-based materials to increase contrast in these images.

Superparamagnetic nanoparticles are an option for an improved contrast enhancement [37]. These particles are generally smaller than 25 nm and exhibit only one magnetic domain and can aggregate in solution to sizes near 200 nm. The aggregates can further improve contrast enhancement but must still remain small enough to migrate into the tissue. Superparamagnetic nanoparticles have the potential to locate individual cancer cells as they metastasize to new

locations in a patient's body. MNPs improve the contrast of MRI by providing more magnetic signal from a smaller amount of magnetic material [37]. If a doctor can visualize the cancer better, there is an increased chance it can be removed or treated before it has a chance to metastasize elsewhere in the body. The localization of the nanoparticles to tumors or cancerous cells can be increased by targeting molecules, such as antibodies, attached to the MNPs.

Other options for imaging and diagnostics include quantum dots and fluorescent tags [1]. These optical visualization techniques offer better spatial resolution than traditional MRI [38]. Quantum dots can be used for cellular imaging and tracking because of their unique optical properties. Because a change in the diameter of the quantum dot alters its emission spectrum, multiple sizes of quantum dots, with different surface functionalities, could be used to image multiple subcellular domains in the same system [1]. One common material used to make quantum dots is cadmium selenide, which is considered toxic; surface modifications are required to increase their biocompatibility [1]. Fluorescently-tagged magnetic nanoparticles can be used for visualization as well [38]. The advantage of this design is that the magnetic nanoparticle can also be used for hyperthermia therapy or as triggers for controlled release of bioactive agents [39].

The benefit of using magnetic nanoparticles for imaging and diagnostics is aligned with the NCI initiative for creating a novel cancer treatment platform. Magnetic nanoparticles are capable of being used pre- and post-treatment as a means for diagnosing the patient, and monitoring the effectiveness of the treatment [14, 39]. The treatment can even be localized by exploiting the magnetic properties of the particles [14, 17]. Further surface modification, through ligands, antibodies, or polymers, can also control the localization or retention of magnetic nanoparticles *in vivo* [2, 14, 17, 39].

2.3 Magnetic Nanoparticles in Living Systems

To apply magnetic nanoparticles into novel treatments for cancer, first the MNPs must be screened for behavior in biological systems. The toxicological properties of a nanomaterial can be vastly different than the bulk properties of the same compound. For example, copper nanoparticles with a diameter of 23.5 nm have been shown to have a median lethal dose (LD_{50}) of approximately 400 mg/kg in mice, whereas copper particles with 17 μm diameters have a value greater than 5000 mg/kg [29, 40]. The LD_{50} represents the dose of a material that results in the death of 50% of the animals tested for a particular administration route; a lower LD_{50} represents a more toxic material. Controlling the properties of nanoparticles is an important step in the development of these novel treatments. The increased surface area to volume ratio of MNPs means that the nanoparticles interact with cells more than larger particles. Size, shape, and composition of the nanoparticle are all properties that can change how a living system interacts with the MNPs [2, 29, 41]. The surfactant, or ligand used to disperse the MNPs in aqueous solutions, can also affect how the biological system will interact with the particles. Common surface coatings used with magnetic nanoparticles for medical applications include 2,3-mesodimercaptosuccinic acid (DMSA), gold, silica, dextran, poly(ethylene glycol), and proteins such as albumin [2].

2.3.1 Toxicity of Magnetic Nanoparticles

The biocompatibility of magnetic nanoparticles is one of the most important properties to be investigated while developing a novel cancer treatment platform. The toxicity and immunogenicity need to be understood before incorporation into treatments that enter a patient's

body. The nanoparticles need to be non-toxic and non-immunogenic, so that they do not harm cells or cause a defensive response from the immune system. Bioaccumulation is another important factor to consider when designing MNPs. The nanoparticles can either accumulate in a specific organ or organ system, such as the liver or be metabolized and removed from the body. The following sections discuss the possibility of MNPs designed to interact with macrophages, as a part of the immune system.

Another important aspect of magnetic nanoparticle toxicity is understanding why some particles may be harmful to cells. A good example of this principle is the difference between necrosis and apoptosis. If nanoparticles kill cells, the mechanism of cell death is important in understanding how to design nontoxic nanoparticles. Apoptosis is a mediated form of cell death where the cell actively and systematically destroys itself by breaking down genetic materials and organelles [42]. On the other hand, necrosis is an immediate form of cell death induced by dramatic stresses on cells [42]. Necrosis caused by magnetic nanoparticles represents a high level of initial toxicity of the MNPs. Because apoptosis is a genetically-controlled process, apoptosis induced by exposure to magnetic nanoparticles could explain the mechanisms of MNP uptake by cells. For example, if the apoptotic processes are initiated after exposure to magnetic nanoparticles, it may be possible that the nanoparticles have bound to specific receptors on the cell surface before being endocytosed. Determining the nature of these receptors would help explain how the nanoparticles are taken into the cell.

The composition of magnetic nanoparticles for medical applications is another important consideration. The most common materials investigated include maghemite, magnetite, and other ferrite-based compounds such as cobalt ferrite. The family of iron oxide particles is considered biocompatible and shows little cytotoxicity [20]. One of the advantages of these

materials is that they are capable of biodegrading *in vivo* as the iron can become incorporated into hemoglobin [20]. Other studies show that $CoFe_2O_4$ exhibits good biocompatibility as well [19, 32, 33, 43]. Even Fe_3O_4 MNPs surface-modified with biotin and labeled with the fluorescent dye fluorescein isothiocyanate (FITC) show negligible toxicity in HeLa cells over extended time periods [44]. HeLa cells are an immortal human cervical cancer cell line established from patient Henrietta Lacks.

2.3.2 Localization of Magnetic Nanoparticles in Living Systems

The localization of nanoparticles in living systems determines cytotoxic properties as well as any potential therapeutic properties. However, this means the tendency for a specific type of cell or tissue to internalize magnetic nanoparticles can be utilized for the design of a treatment platform. The route of exposure can also affect the *in vivo* behavior of a nanoparticle [29]. For example, inhaled nanoparticles can remain in the respiratory tract of humans for approximately 700 days, while ingested NPs are excreted through urine and feces much more quickly [29]. Size is another important consideration in the study of nanoparticle localization. If particles are smaller than 10 nm in diameter, they are easily rapidly cleared from the body by the kidneys [2]. On the other hand, if the particles are larger than 200 nm they can activate the reticuloendothelial system in the liver and spleen, which removes the particles from circulation [2].

The different levels of localization of MNPs in living systems correspond to the organization of the biological systems investigated. In mouse studies, nanoparticles have been reportedly found in the liver, spleen, kidneys, brain, and lungs after an oral exposure to gold nanoparticles [29, 45, 46, 47]. Smaller particles were more widely dispersed throughout the

body, while larger particles remained in the GI tract [45, 46]. Another study showed similar results, with Au-Au_2S nanoparticles remaining localized to the liver and spleen of mice 7 days after intravenous injection [48]. Fabian et al. have shown that TiO_2 nanoparticles approximately 20 nm in diameter are mostly cleared from the lungs, kidneys, and spleen of mice within 28 days [49]. The localization of nanoparticles to the liver and spleen represents the natural defense of the reticuloendothelial system.

On the cellular level, nanoparticles are most likely to be internalized by macrophages [20, 29, 50]. Because macrophages are a part of the defense system, they recognize nanoparticles are foreign agents and remove them from circulation. According to several studies, macrophages can take up dextran-coated iron oxide nanoparticles, which remain in endosomes [20, 51]. In HeLa cells, internalized iron oxide nanomagnets functionalized with biotin and FITC were shown to be localized to lysosomes [44]. In fibroblasts, internalized Fe_3O_4 nanoparticles coated with poly(ethylene glycol) had little effect on the structure of the microfilaments of the cytoskeleton [3]. In the same study, uncoated MNPs were shown to disrupt the cell membrane and cytoskeleton of fibroblasts [3]. The mechanisms of nanoparticle uptake into cells are mentioned in the following section.

2.3.3 Uptake Mechanisms of Magnetic Nanoparticles

The general mechanisms of cellular internalization are collectively known as endocytosis. Endocytosis is a process by which the cell membrane envelops the particle to be internalized, before pinching off into the cytoplasm of the cell. The resulting organelle is called an endosome, the membrane of which is made of the same materials as the cell's plasma membrane. The endosome may then be localized to other organelles depending on the endocytosed material.

Foreign matter or food particles are usually delivered to lysosomes to be degraded by hydrolytic enzymes. Endocytosis is typically subdivided into pinocytosis and phagocytosis. Pinocytosis is the internalization of liquids or particles less than 300 nm in [52]. Phagocytosis is the method of uptake for particularly large particles, with size range 0.25 to 10 μm [52]. Endocytosis can be nonspecific or receptor-mediated, depending on the surface of the particles being taken up [51, 52].

Once introduced into a biological system, the most common places for magnetic nanoparticles to be absorbed by are macrophages and endothelial tissues [51]. These cells and systems act as protective agents, separating the native components of the body from foreign agents. The most commonly studied target of MNPs is macrophages [20, 51, 53]. Because of their role as scavengers and defense cells, they naturally target the non-native magnetic nanoparticles and remove them from the body. This property can be exploited as a part of a targeting platform. Macrophages actively internalize a variety of negatively charged particles [51]. Most research indicates that either nonspecific or receptor-mediated endocytosis is the process by which nanoparticles are internalized by cells [51, 53, 54].

Determining the mechanisms by which cells internalize MNPs is an important aspect of designing novel nano-based therapeutic devices. Wilhelm has studied the process of magnetic nanoparticle uptake in HeLa cells [50, 53]. These studies have been successful at showing a two-step mechanism for the internalization of maghemite nanomagnets in both mouse macrophages and HeLa cells. The magnetic nanoparticles were dispersed in water using 2,3-mesodimercaptosuccinic acid. In the first step, the anionic coating of the magnetic nanoparticles interacted with the plasma membrane of the cells, adsorbing to the surface. In the second step, the Fe_2O_3 particles were endocytosed into the cell. The research by Wilhelm shows

quantitatively the relation between magnetic nanoparticle uptake and cell type. Another study performed by Wilhelm shows that anionic maghemite nanoparticles have an increased affinity for cellular uptake in HeLa cells and mouse macrophages, as opposed to neutrally-charged dextran-coated iron oxide particles [53]. Coating the nanoparticles with the negatively-charged protein albumin inhibits their uptake into cells. In their study, Becker et al. found that HeLa cells endocytosed Fe_3O_4 magnetic nanoparticles that have been functionalized with biotin and labeled with FITC [44]. Because the nanoparticles were primarily localized into lysosomes, endocytosis is supported as the mechanism of uptake for these MNPs as well.

By varying the surface coating of magnetic nanoparticles, the cellular uptake can be controlled. Research has shown that unspecific endocytosis is responsible for the rapid uptake of dextran-coated magnetite or aminosilan-coated magnetite particles in a variety of cancerous and normal cell lines [55]. Because the magnetic nanoparticles were coated in polymers that did not activate any of the receptors on the cell surfaces, the same nonspecific mechanism must be responsible for the uptake of the nanoparticles. The same study shows increased uptake in cancerous cells as opposed to normal cells; this is interpreted as meaning that quickly dividing cells can internalize magnetic nanoparticles more efficiently than slower dividing counterparts. However, other studies have indicated that a receptor-mediated endocytosis process may be utilized in magnetic nanoparticle uptake. Macrophage uptake of dextran-coated iron oxide nanoparticles can also be controlled by adjusting the concentrations of different factors involved in cellular processes [54]. Increasing the concentrations of an anti-inflammatory cytokine, interluekin-4, increases the amount of iron oxide internalized by mouse macrophages grown in culture. In the same study, the effects of increasing the concentration of the reductase inhibitor lovastatin decreased the amount of MNPs endocytosed by the cells. The exclusion of fetal

bovine serum also decreases the amount of magnetic nanoparticles endocytosed by the cells. Increasing concentration of cytokines, which regulate the levels of receptor activation on the macrophages, enhanced the uptake of dextran-coated magnetite into the macrophages.

Because surface functionality, size, and cell type can affect the manner in which magnetic nanoparticles are internalized, additional studies are needed to determine the optimal design of the proposed treatment system. The mechanism of internalization and toxicological properties of $CoFe_2O_4$ magnetic nanoparticles labeled with the fluorescent dye rhodamine B were investigated in this project. To better understand the interactions between magnetic nanoparticles and biological systems, samples of $CoFe_2O_4$ were tagged with a fluorescent dye before being introduced into different biological systems including HeLa cells and *Caenorhabditis elegans* (*C. elegans*) worms. The uptake and localization, as well as toxicity, were studied in these systems.

Chapter 3

SIGNIFICANCE

This project is an important focus of the overall goal of improving cancer therapy through use of magnetic nanoparticles. Current cancer treatment methodologies including radiation, surgery, and chemotherapy all utilize a “shotgun” approach to killing the tumor. For example, by overwhelming a patient’s system with an anti-cancer drug, there is an increase in the negative side effects experienced by patients because treatments do not discriminate between healthy and cancerous cells. There are several current treatments that are targeted, including radiation therapy and the anti-cancer agent Herceptin. The latter is a recombinant humanized monoclonal antibody that targets the extracellular portion of a protein expressed in breast cancer cell membranes and can be used in combination with chemotherapy agents doxorubicin and paclitaxel [56]. This combination of Herceptin and anti-cancer therapeutic has been shown to increase survival and treatment-response rates in cancer patients, but can lead to severe cardiovascular side effects [56]. However, additional work is needed to create an optimal targeted and localized treatment platform, which would help reduce such negative side effects.

The combination platform proposed by the Magnetic Biomaterials Research group is a thermally-responsive hydrogel embedded with magnetic nanoparticles. The magnetic nanoparticles can be heated using an external magnetic field. As the particles heat, they cause a thermal response in the gel which in turn controls the release of an anti-cancer therapeutic. The complementary action of localized heating and drug release offers a unique way for combination

therapy of hyperthermia and chemotherapy. The magnetic nanoparticles can be placed using a static magnetic field and externally triggered via exposure to a high frequency magnetic field. Including the magnetic nanoparticles offers a way to localize and externally-trigger the treatment, which will also help increase efficacy and improve quality of care.

Using nanoparticles in the cancer treatment platform is one way to target and control the delivery of an anti-cancer therapeutic. Because nanotechnology is so new, the interactions between biological systems and nanoparticles are not completely understood. Polymer systems have been studied *in vivo* for some time, with some systems, for example poly(lactic-co-glycolic acid), showing a high degree of biocompatibility [57]. So the goal of this project is to improve the understanding of how magnetic nanoparticles, the novel entity in the combined platform, interact with living systems. This project fits into the comprehensive goal of improving cancer therapy by understanding how magnetic nanoparticles interact with and localize to different types of cells. Through understanding these behaviors, we can design nanoparticles with minimal *in vivo* toxicity but effective tumor-targeting abilities.

Chapter 4

OBJECTIVES

The overarching purpose of this project was to characterize the behavior of magnetic nanoparticles in biological systems. An important aspect of any nanomedical platform includes understanding how the physical properties of the nanoparticles, such as composition, size, and surfactant, affect *in vivo* behavior of nanoparticles, including, localization, internalization, bioaccumulation, and cytotoxicity. This project looks at determining some of these behaviors of magnetic nanoparticles in model biological systems, so that the materials may be incorporated into larger projects designing the treatment platform.

My specific goals in this project were the following:

A. To synthesize and characterize cobalt ferrite ($CoFe_2O_4$) magnetic nanoparticles
B. To label $CoFe_2O_4$ magnetic nanoparticles with the fluorescent dye rhodamine B
C. To introduce rhodamine-tagged $CoFe_2O_4$ to two different model biological systems and study the uptake and localization of the particles
D. To determine toxicity of rhodamine-tagged and rhodamine-free $CoFe_2O_4$ nanoparticles in biological systems

Chapter 5

MATERIALS AND METHODS

This section contains a description of the methods used to synthesize cobalt ferrite MNPs and tag them with the fluorescent dye rhodamine. The procedures used in HeLa cell localization studies are outlined, as are the methods to determine toxicity of MNP solutions in HeLa cells. Additionally, the description of the procedures used in MNP localization studies in *Caenorhabditis elegans* worms is discussed.

5.1 Synthesis of Rhodamine-Tagged $CoFe_2O_4$

Samples of $CoFe_2O_4$ were synthesized in-house using the method developed by Sun *et al.* [58]. Briefly, in a round-bottom flask, 2 mmol of iron (III) acetylacetonate, $Fe(acac)_3$ (Acros Organics, Morrison Plains, NJ), and 1 mmol of cobalt(II) acetylacetonate, $Co(acac)_2$ (Acros Organics, Milwaukee, WI), were mixed with 10 mmol of 1,2 hexadecanediol (Aldrich Chemical Company Inc., St. Louis, MO), and 20 mL benzyl ether (Acros Organics, Morrison Plains, NJ). Also included were 1.90 mL oleic acid (Fisher Scientific, Fair Lawn, NJ) and 2.05 mL oleylamine (Acros Organics, Morrison Plains, NJ). The solution was magnetically stirred under nitrogen and refluxed at 200 ^{o}C for 2 h, then heated to 300 ^{o}C and refluxed for an additional hour. After cooling, ethanol was added to the sample before centrifugation at 2000 rpm for 20 min to precipitate the solid product. The ethanol wash and centrifugation was repeated, and then the sample was dried under nitrogen before being dispersed in approximately 20 mL of hexane

(Acros Organics, Morrison Plains, NJ). The procedure yielded $CoFe_2O_4$ magnetic nanoparticles which were easily dispersed in hexane with diameters ranging from 7 to 10 nm. To disperse the $CoFe_2O_4$ in water, a ligand exchange reaction was conducted. The surfactant used to disperse the MNPs in water was 2,3-mesodimercaptosuccinic acid (DMSA) (Sigma Chemical Company, St. Louis, MO). First 5.0 mL $CoFe_2O_4$ in hexane were mixed with 5.0 mL dimethylsulfoxide (DMSO) (Fisher Scientific, Fair Lawn, NJ). To this solution, 20 mg of DMSA were added. The procedure could be scaled up or down, depending on the desired volume and relative concentration of the aqueous solution. The mixture was sonicated overnight. The MNPs in the inorganic layer were pipetted out and diluted with deionized (DI) H_2O. For a solution that started as 5.0 mL $CoFe_2O_4$ in hexane, approximately 10 mL of water were needed to achieve a stable dispersion of the MNPs. This number varied according to the desired volume and relative concentrations needed for the characterization and cell culture studies.

The aqueous dispersions of $CoFe_2O_4$ were further modified by the addition of a fluorescent dye, rhodamine. The tagging procedure is described elsewhere by Bertorelle *et al.* [38]. Briefly, samples of $CoFe_2O_4$ dispersed in water using DMSA as a ligand were mixed in a 1:3 volume ratio with a rhodamine-thiol dye solution for three hours. The dye solution contained 17 mg rhodamine B (ICN Biomedicals Inc., Eschwege, Germany), 4 mg cystamine (Acros Organics, Morrison Plains, NJ), and 7 mg of 1-ethyl-3-(3-dimethylaminopropyl) carbodiimide (EDC) (Pierce, Rockford, IL) in 20 mL of DI water. After stirring, the sample was rinsed twice with DI water, using a neodymium magnet to separate and hold the MNPs in place during decantation. The MNPs were then diluted to a total volume of 15 mL using DI water. Tetramethylammonium hydroxide (TMAOH) (Fisher Scientific, Fair Lawn, NJ) was added to bring the solution pH to roughly 10 before the sample was stirred for 45 minutes. Afterwards,

1.0 N hydrochloric acid (HCl) (Acros, Morrison Plains, NJ) was added to adjust the pH to approximately 7. To cause the MNPs to fall out of solution, 0.1 mg sodium chloride (NaCl) (EM Science, Gibbstown, NJ) was added for every mL of solution. A neodymium magnet was used to separate the MNPs from solution so the excess rhodamine could be washed away. The sample was successively washed with DI water until the supernatant became clear. Sample analysis followed. The accepted reaction pathway for the rhodamine-tagging process involves the dye attaching to the surface of a MNP coated in DMSA via a thiol bond (Figure 5.1). In the following sections $CoFe_2O_4$ samples of MNPs with the rhodamine dye will be designated as rhodamine-tagged, while samples that are dispersed in water, but do not have the dye, will be referred to as untagged.

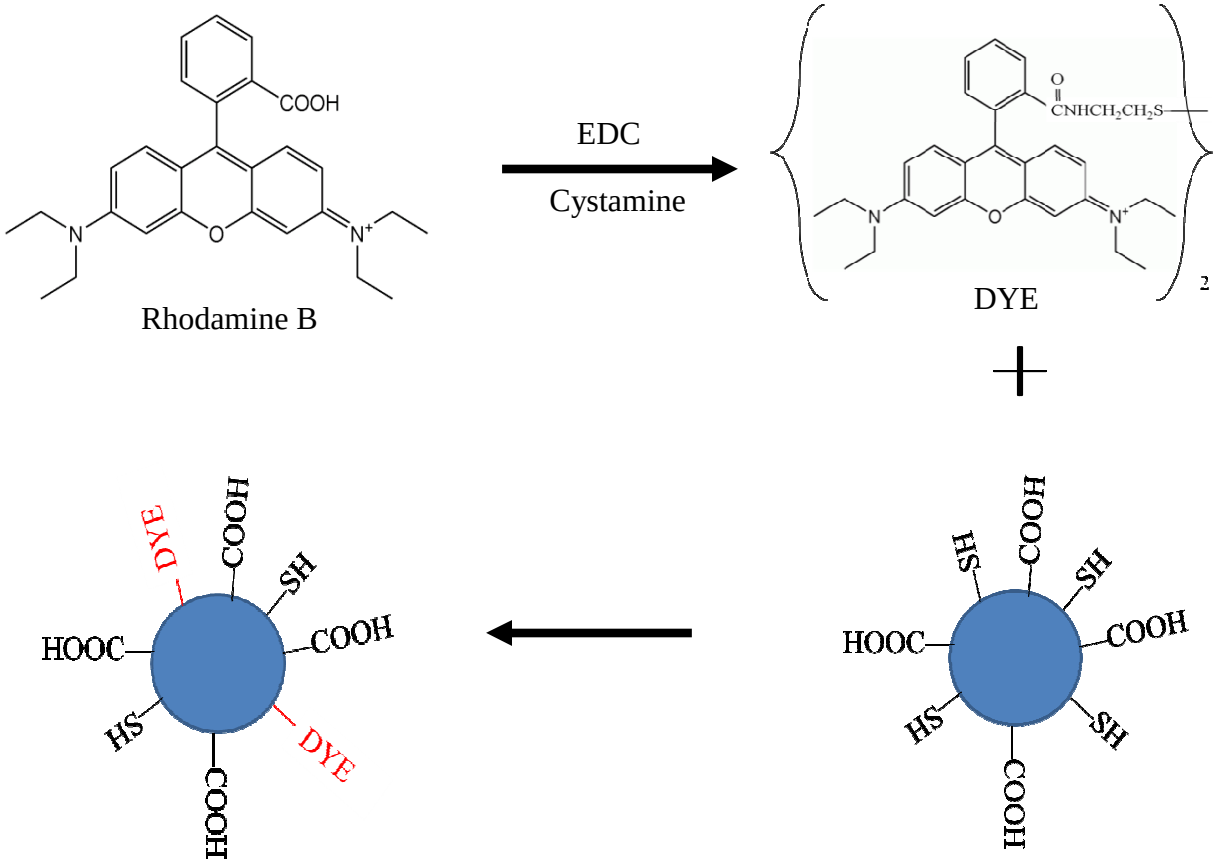

Figure 5.1 Schematic of Reaction that Attaches Rhodamine B to $CoFe_2O_4$ MNPs. Rhodamine Dye Attaches via a Thiol Bond to MNPs Dispersed in Water with the Surfactant DMSA. When the Dye is Reacted with the $CoFe_2O_4$ MNPs, the Dye Dimer Splits between the Two Sulfurs, These are the Sulfurs in the Thiol Bond to the MNP Surface. Adapted from [38].

5.2 Analysis of $CoFe_2O_4$ Magnetic Nanoparticles

After synthesis, the untagged $CoFe_2O_4$ and rhodamine-tagged $CoFe_2O_4$ samples were analyzed to determine concentration and particle size. To determine concentration, first an aluminum crucible was weighed using a microbalance. A known volume of MNP sample was added to the crucible before being placed in an oven at 50 ^oC to dry overnight. After a 24-hour drying period, the solution and crucible were massed. The difference was divided by the sample volume, giving the concentration in mg of MNPs per mL of solution.

Dynamic light scattering (DLS) was used to determine the particle size. To determine nanoparticle diameter, a Nano-sizer ZS (Malvern Instruments Limited, Westborough MA) was used. All samples were assumed to have the same refractive index as water (n=1.33). The position of the attenuator and correlation function for each sample were determined using the optimization properties of the DLS software. Prior to analysis, each sample was sonicated for 24 hours. Table 5.1 identifies samples analyzed by these methods. In addition to sonication, Samples 1-6 were filtered using Poretics® polyester 0.4 μm syringe filters (Osmonics, Inc., Minnetonka, MN). During the filtering process, up to 1.5 mL of solvent, hexane for Sample 1 and DI H_2O for all other samples, were added to solutions to counteract the caking effects on the filter. Samples A to F were not filtered, to maintain sample concentration. In this study, it was important to ensure the concentrations mimicked concentrations used in several of the cell culture studies.

Table 5.1 Sample IDs and Descriptions for $CoFe_2O_4$ Magnetic Nanoparticle Solutions

Sample ID	Solvent	Surfactant	Date Synthesized
1	Hexane	Oleic Acid	02-03-09
2	DI H_2O	DMSA	04-01-09
3	DI H_2O	DMSA	04-01-09
4	DI H_2O	DMSA, Tagged with rhodamine	04-08-09
5	DI H_2O	DMSA	02-07-09
6	DI H_2O	DMSA	11-13-08

5.3 Toxicity of $CoFe_2O_4$ MNPs in HeLa Cells

A toxicity screening of the rhodamine-tagged $CoFe_2O_4$ and untagged $CoFe_2O_4$ samples described in the above section was performed using HeLa cells. The dilutions of MNPs tested were 1, 2.5, 5, 7.5, and 10 vol% in media, which correspond to a concentration range of 0.005 to 0.05 mg/mL (Table 6.3). A negative control, 0 vol% MNPs, and a positive control 10 vol% (0.12 g/mL) H_2O_2 in media, were also used. The experimental setup was a 96-well plate, with each row being used for a different concentration of MNPs. The first seven rows contained cells and media, while the bottom row contained only MNP solutions. Cells were incubated in the well plates at 37 ^oC and 5% CO_2 for 24, 48, or 93 hours. The experiments were performed in quadruplicate. Figure 5.2 shows the experimental setup used in the toxicity studies.

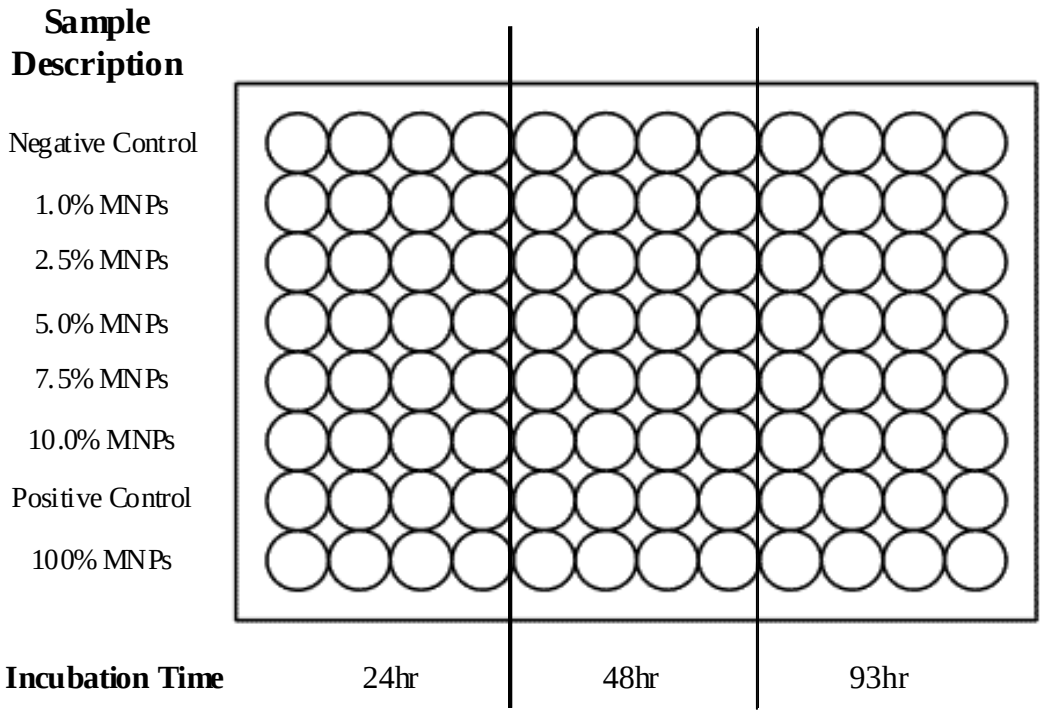

Figure 5.2 Experimental Setup in $CoFe_2O_4$ MNP Toxicity in HeLa Cell Studies.

The 96-well plate was first loaded with 100 μL of media containing roughly 5,000 cells per well. Next, solutions of MNPs in media were added to each of the wells. Both MNP solutions were sonicated for 30 min prior to mixing with media. The total volume in each of the wells after the addition of the MNP solutions (or an equal volume of media for the wells with no MNPs) was 110 μL. The plates were incubated at 37 ^{o}C and 5% CO_2 for the specified time period.

Viability assays were performed using a CellTiter® Aqueous Cell Proliferation Assay (Promega, Madison, WI). The assay reagent used was 3-(4,5-dimethylthiazol-2yl)-5-(3-carboxymethoxyphenyl)-2-(4-sulfophenyl)-2H-tetrazolium salt (MTS) mixed with an electron coupling agent, phenazine ethosulfate (PES), in a 20:1 volume ratio. After the incubation time, 20 μL of the assay reagent was added to each of the wells to be analyzed for that time period. The well plates were incubated for another hour before being read on an ELISA 96-well plate reader. Absorbance for each well was measured at 490 nm, this correlated to the cell density in the wells. The well plates were then placed back in the incubator for the continuing time period of the study.

5.4 Localization of Rhodamine-Tagged $CoFe_2O_4$ in HeLa Cells

To determine cellular localization of magnetic nanoparticles, HeLa cells (ATCC CCL-2, obtained from the Gene Therapy Lab of Dr. Maaike Everts at the University of Alabama in Birmingham) were exposed to rhodamine-tagged $CoFe_2O_4$ for various time periods. The cells were grown in a 1:1 volume ratio solution of Dulbecco's modified Eagle's medium and Ham's F12 medium (Mediatech, Herndon, VA) with 10% fetal bovine serum (Hyclone, Logan, UT), L-glutamine (2nm, Mediatech, Herndon, VA), penicillin (100 IU/mL, Mediatech, Herndon, VA),

and streptomycin (25 μg/mL, Mediatech, Herndon, VA) and incubated at 37 ^{o}C and 5% CO_2. The internalization time periods tested were 2 hours, 6 hours, and 24 hours. The concentration of MNPs was 10 volume percent in media. This concentration was chosen because it represents the limiting concentration of any "non-media" solution incorporated into cell culture media without limiting the diffusion of nutrients to the cells [59]. A 30 min time period was also tested at different concentrations of MNPs: 1 vol% rhodamine-tagged $CoFe_2O_4$, 10 vol% untagged $CoFe_2O_4$, and a negative control (no MNPs). Before dilution with media, the tagged samples in this case had an initial concentration of either 0.60 mg/mL or 0.54 mg/mL, and the untagged MNPs had an initial concentration of 5.06 mg/mL. Two replicates of each concentration were incubated.

The cells were transferred from a tissue culture flask to either a two- or eight-well chamber slide roughly 24 h before the experiments took place. The 30 min samples had an initial cell concentration of approximately 50,000 cells/well. The cultures were washed twice with phosphate buffer solution (PBS) (Fisher Scientific, Fair Lawn, NJ) before the media containing MNPs was added to the wells. The cultures containing MNPs were incubated at 37 ^{o}C and 5% carbon dioxide (CO_2) for the specified time periods before staining and imaging.

Immediately after incubation, the HeLa cell cultures containing MNPs were washed twice with PBS before being stained with phalloidin (Alexa® Fluor 488 phalloidin, Invitrogen, Carlsbad, CA). This particular phalloidin is a green-fluorescing actin filament stain that can be used to visualize the cell membrane and was chosen because the coloration exhibit minimal interference with the excitation or emission spectra of the rhodamine-tagged MNPs. After it was received, the phalloidin stain was dissolved in 5 mL of methanol (Acros Organics, Morrison Plains, NJ) to create a stock solution. After incubation, the HeLa cultures (with and without

MNPs) were submerged in and fixed using 3.7% formaldehyde (Fisher Scientific, Fair Lawn, NJ) in PBS solution for 10 min and then washed two more times with PBS. Samples were submerged in 0.1% Triton-X (Aldrich Chemical Company Inc., Milwaukee, WI) in PBS for 5 minutes and then washed twice with PBS. Each chamber was submerged in a 1:40 volume dilution of phalloidin-methanol stock solution in PBS for 20 min and then washed twice with PBS. A more complete description of the staining procedure is given in Appendix 1.

Following phalloidin staining, the samples were stained with Hoechst 33342 (Molecular Probes (Invitrogen), Eugene, OR). Hoechst is a nuclear stain which fluoresces blue, so that there would be minimal interference with the phalloidin and rhodamine. The cultures were soaked in a $5x10^{-4}$ mg/mL solution of Hoechst in PBS for 2 min, before being washed twice with PBS. Then the samples were embedded using an anti-fading agent before the well chamber piece was removed, leaving only the slide with the fixed cultures. The slides were imaged using an Olympus IX70 fluorescence microscope (Olympus America Inc., Center Valley, PA) as well as a Leica TCS SP2 confocal laser scanning microscope (Leica Microsystems, Bannockburn, IL) to determine localization of MNPs within the cells. Images were collected using lasers at 488 nm to excite the Alexa 488 phalloidin stain or 543 to excite the rhodamine, resulting in green and red images which could be superimposed to determine the relative positions and colocalization of MNPs and cell membranes.

5.5 Toxicity and Fluorescence Imaging Studies of Rhodamine-Tagged $CoFe_2O_4$ MNPs in *C. elegans* Worms

Caebhnoris elegans worms (obtained from a laboratory at The University of Alabama) were used as a model organism for magnetic nanoparticle localization studies. In these studies, both wild type worms and mutant worms were studied. *C. elegans* was selected as a model

organism for two reasons. The first is because *C. elegans* are one of the few organisms whose entire genome is fully known and well studied as a model organism. Also, the worms represent a multi-cellular organism to give an idea how MNPs may localize or bioaccumulate in higher organisms. The mutant worms contained genes causing neurons to fluorescence green. The experimental setup included a Petri dish containing agar with an OP50 bacterial lawn and eight to ten L4 (young adult) worms. The bacterial lawn contained a streptomycin resistant *Escherichia coli* strain, which acts as a common food source for *C. elegans*. To the Petri dish, 200 μL of rhodamine-tagged $CoFe_2O_4$ solution were added. The sample of MNPs was synthesized on 0-2-10-09, had an average peak diameter of 250 nm, and had a concentration of 0.54 mg/mL. The samples were allowed to grow for two days before being analyzed. Experiments were repeated in triplicate. The mutant worms were allowed to grow in media containing MNPs for two time periods: 24 h and 12 days. The toxicity of rhodamine-tagged $CoFe_2O_4$ to *C. elegans* worms was determined qualitatively by monitoring whether or not the worms were capable of reproduction.

Chapter 6

RESULTS AND DISCUSSION

The following section discusses the analyzed properties of the rhodamine-tagged $CoFe_2O_4$ magnetic nanoparticle solutions, including concentration and average peak diameters. Information is also included regarding the stability of these solutions and the tendency of the MNPs to aggregate. Afterwards, the results from MNP localization and toxicity studies in HeLa cells are outlined. The rhodamine-tagged $CoFe_2O_4$ nanoparticles were localized in the cytoplasm of the cells and showed negligible toxicity at concentrations at or below 5 vol% MNPs in media.

6.1 Characterization of $CoFe_2O_4$ Magnetic Nanoparticles

After synthesis, the samples of rhodamine-tagged and untagged $CoFe_2O_4$ magnetic nanoparticles were characterized to determine concentration and particle size. The stability of the attachment of the rhodamine dye to the surface of the MNPs was also investigated. A solution of rhodamine-tagged $CoFe_2O_4$ was analyzed to determine whether or not the rhodamine dye is capable of detaching from the surface of the MNP over time. The solution had an approximate concentration of 0.05 mg/mL. The solution was diluted from Sample 4 (Table 6.2) on 06-23-09. The sample was sonicated overnight before being placed on a neodymium magnet for 30 min to force the MNPs out of solution. The absorbance of the supernatant was measured at 553 nm using a Shimadzu UV-2401 spectrometer (Shimadzu Scientific Instruments, Columbia, MD). The absorbance was first measured for a sample that

had been at room temperature prior to analysis. After sonication overnight, a second sample of rhodamine-tagged MNPs at the same concentration was placed in a hot water bath at 37 ^{o}C for 24 h. Afterwards, the sample was placed on the neodymium magnet for 30 min before absorbance was measured at 553 nm.

The concentration of free rhodamine in solution was related to the concentration of MNPs in the sample and the sample volume. For the room temperature solution, there was 0.01 mg free rhodamine dye for every mg of $CoFe_2O_4$ MNPs. For the sample which had been held at 37 ^{o}C for 24 h, there was also 0.01 mg free rhodamine dye per mg MNPs, indicating that the MNP-rhodamine chemical bond is stable in aqueous solution. However, this study did not fully reflect the conditions the MNPs would encounter in biological systems. A study of the stability of the rhodamine attachment to $CoFe_2O_4$ MNPs in media is recommended. This would determine whether or not the dye remains attached to the MNP in the presence of amino acids and proteins which could interfere with the thiol bond between the dye and the MNP. Another factor that could have influenced these results is the age of the solution. Sample 4 was synthesized approximately two months before this analysis was completed. The time between synthesis and analysis could have allowed for the dissociation of some of the rhodamine from the surface of the $CoFe_2O_4$ particles. Free rhodamine dye in the solution could be internalized by cells and would cause red fluorescence to be visualized when the MNPs may not have been internalized. Additional work is needed to determine the stability of the rhodamine-MNP bond. Data and sample calculations from these experiments are included in Appendix 2.

The results from dynamic light scattering analysis indicate the $CoFe_2O_4$ MNPs tend to aggregate in solution. The smallest measured average diameter was approximately 100 nm, while older samples showed agglomerates up to 5,500 nm in diameter. Although the aqueous-

dispersed samples of $CoFe_2O_4$ tended to form aggregates, this is a common problem in MNPs for medical applications [2, 23, 55]. The agglomeration is thought to be caused by instability introduced into the solution because of the hydrophobic- nature of the MNPs after synthesis and attractive magnetic forces.

A possible explanation of the instability could be that the ligand exchange with DMSA is not highly efficient, which would lead to residual organic soluble ligands on the surface of the MNPs. After synthesis, the MNPs are coated in a layer of organic soluble ligands; as a result, MNP aggregates will try to form so that hydrophobic portions of the nanoparticle surface are held away from the aqueous environment. This causes additional aggregates due to the increased magnetic forces between aggregates. As MNPs cluster, the magnetic force becomes greater, pulling in more MNPs to the agglomeration in a self-perpetuating process [15]. A balance between the dispersing forces of the surfactant and the attractive magnetic forces between the nanoparticles prevent the solution from becoming one large aggregate formed of all the MNPs. The effects of solvent type and sample age on average peak diameter were studied, as described below. Results from the DLS analyses of rhodamine-tagged and untagged $CoFe_2O_4$ MNPs are from samples dispersed in DI H_2O. Because the MNPs are in an aqueous environment the DLS is able to measure the hydrodynamic diameter of the particles. When dispersed in cell culture media, the MNPs may exhibit different sizes due to interactions with proteins and amino acids in the media. Therefore, there is a possible discrepancy between particle diameters reported below and effective particle diameter during the cell culture experiments. Samples of rhodamine-tagged $CoFe_2O_4$ in the media used for the HeLa cells studies (detailed in Section 5.3) analyzed using DLS gave no reliable size data due to interference of proteins with the equipment.

Because an efficient technique to determine MNP diameter in cell culture media was not available, only results from the analysis of aqueous dispersions are presented below.

The size distribution of particles varied depending on the solvent in which the MNPs were dispersed and whether or not rhodamine was tagged to the $CoFe_2O_4$ MNPs (Figure 6.1). Sample 2 showed a larger peak diameter than Sample 1, even though Sample 1 was used to synthesize Sample 2. The MNPs in hexane tend to be smaller than the MNPs in water even after the ligand exchange with DMSA, indicating less stability in aqueous solutions. However, Sample 4 showed a smaller average peak diameter than either Sample 1 or 2. This indicates that the addition of the rhodamine dye to the surface of the MNPs decreases their tendency to aggregate and thus reduces their average peak diameter as measured by DLS. These results also suggest that the rhodamine on the surface of the $CoFe_2O_4$ magnetic nanoparticles helps reduce the tendency to form aggregates in aqueous solutions.

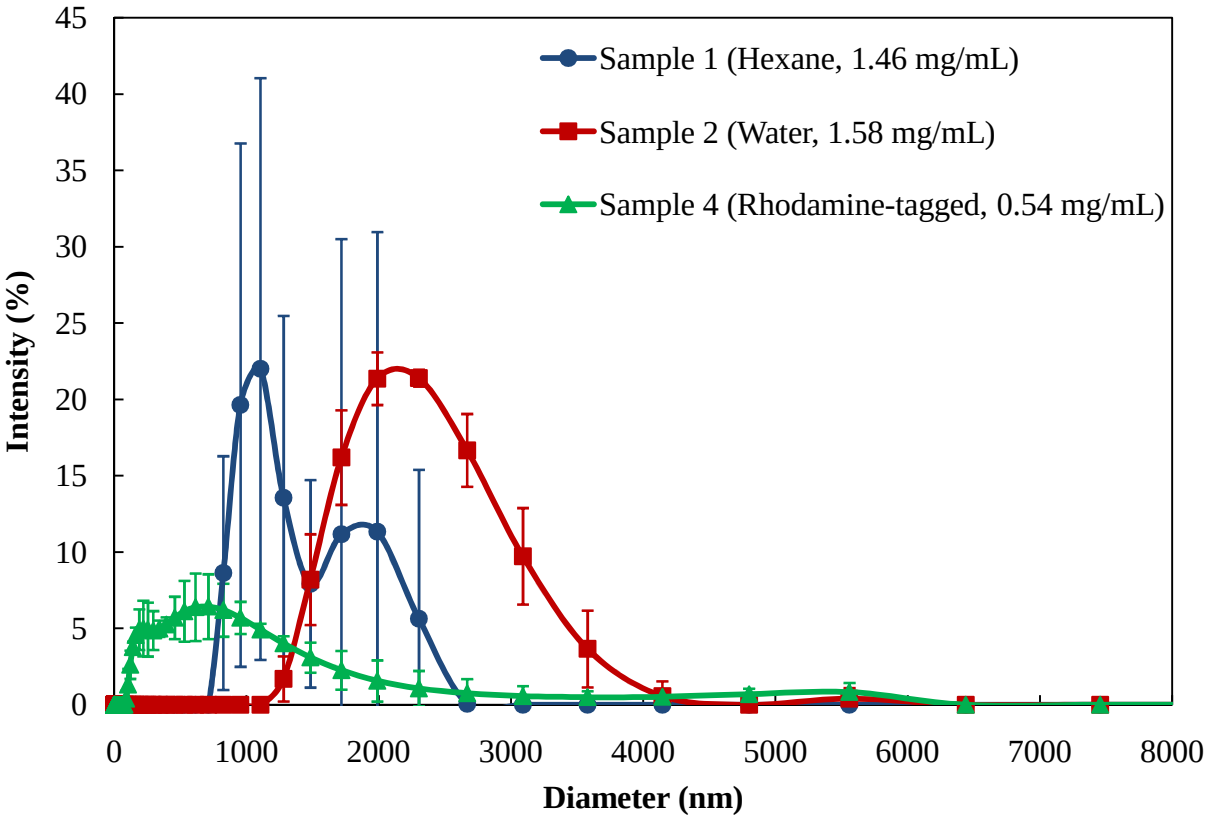

Figure 6.1 Comparison of Solvent Effects on $CoFe_2O_4$ Particle Size. Sample IDs are taken from Table 6.1. Error Bars Indicate Standard Deviation for Three Samples. Where Not Shown, Error Bars are Smaller Than the Data Symbols.

A correlation between concentration, sample age, and average peak particle diameter was also seen. Table 6.1 shows how the concentrations of the MNP solutions in different solvents affected the average peak diameters of the MNP agglomerates. As the concentration of an MNP sample increased, so did the average peak diameter. The same trend was seen in relation to sample age: an older sample exhibited larger diameters and less stability than a newer sample. Samples over four to six weeks old tend to be less stable than newer samples, as confirmed by DLS analysis of particle size. Samples 1 and 2 had similar concentrations and differed only in solvent and date of synthesis. In this instance, the solvent effects on particle size were more drastic than the age of the sample. Samples 5 and 6, which were both $CoFe_2O_4$ dispersed in water using DMSA and had lower concentrations than Sample 2, showed much larger particle diameters and therefore less stability. These two samples were considerably older than Sample 2. Sample 3 was synthesized at the same time as Sample 2 and differed only in concentration of $CoFe_2O_4$ (Figure 6.2). Sample 4 was approximately the same age as Samples 2 and 3 and showed a smaller average peak diameter, again indicating the addition of rhodamine helps stabilize the MNPs in aqueous solutions.

Table 6.1 Effect of Solvent, Rhodamine Attachment, and Sample Age on Sizes of $CoFe_2O_4$ Magnetic Nanoparticle Agglomerates

Sample ID	Solvent	Date Synthesized	Concentration (mg/mL)	Peak Diameter (nm)
Sample 1	Hexane	02-03-09	1.46	1100, 1850
Sample 2	DI H_2O	04-01-09	1.58	2140
Sample 3	DI H_2O	04-01-09	0.58	1280, 5500
Sample 4	DI H_2O (+Rhodamine), Synthesized from Sample 2	04-08-09	0.54	615
Sample 5	DI H_2O	02-07-09	0.92	2300,5500
Sample 6	DI H_2O	11-13-08	0.72	5550

Note: Samples 1 to 6 were analyzed on 05-06-09.

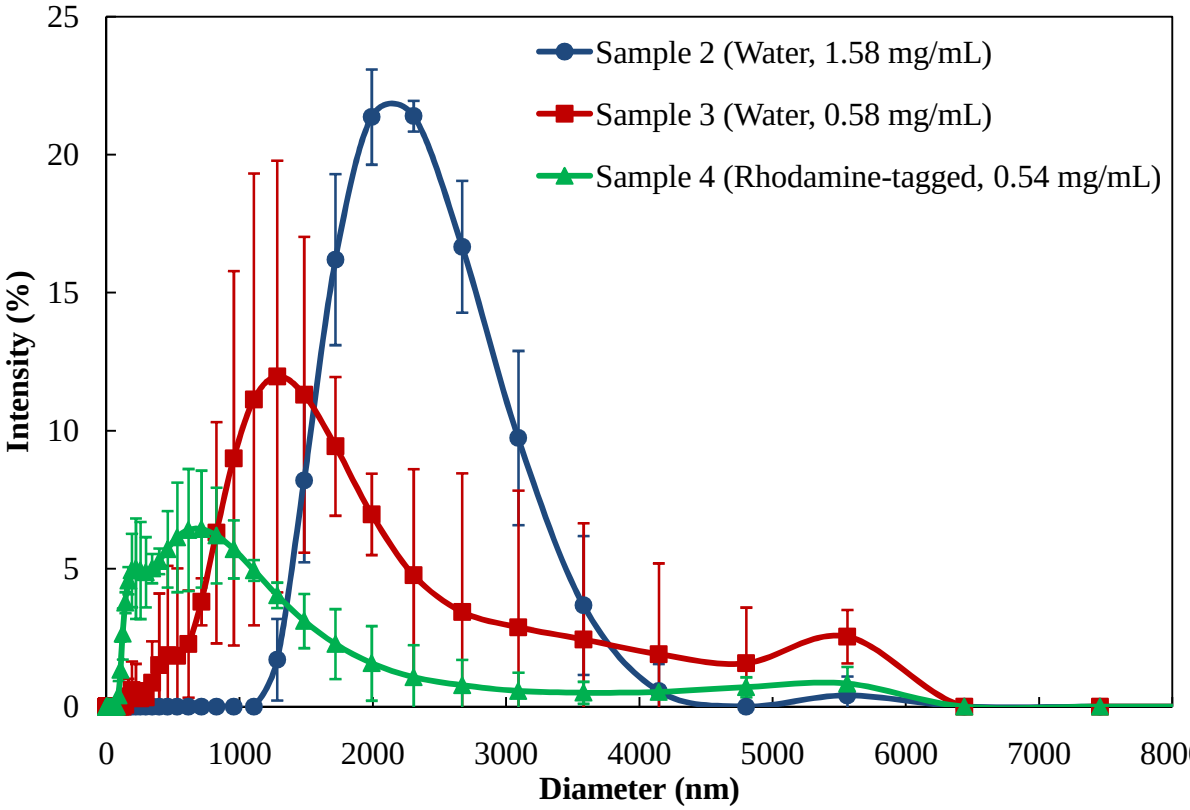

Figure 6.2 Comparison of Concentration Effects and Addition of Rhodamine Dye on $CoFe_2O_4$ Particle Diameters. Error Bars Indicate Standard Deviation for Three Samples. Where Not Shown, Error Bars are Smaller Than the Data Symbols.

DLS analysis was completed on aqueous MNP dispersions that mimicked the *in vitro* concentrations used in the HeLa cell toxicity and internalization studies. From Table 6.1, Samples 4 and 5 were diluted with DI H_2O to create Samples A to F. The concentrations and sample IDs for this study can be found in Table 6.2. Particle size analysis on these samples also shows the importance of concentration on the size of the MNPs in solution. Samples A, B, and C were dilutions of Sample 5; the 1, 5, and 10 vol% dilutions show much smaller average diameters than the undiluted solution. Samples D, E, and F were dilutions of Sample 4, and they also show decreased average particle size. Figure 6.3 shows the differences in Samples A, B, and C while Figure 6.4 shows the difference in sizes in Samples D, E, and F. These results indicate that rhodamine-tagged MNPs have average diameters of approximately 100 nm. Nanoparticle sizes in the range of 100-200 nm are typical for magnetic nanoparticles in aqueous solutions [60]. In those studies, iron oxide MNPs had hydrodynamic diameters ranging from 107-240 nm.

Table 6.2 Sample IDs and Effect of Concentration on Sizes of Dilute $CoFe_2O_4$ Magnetic Nanoparticle Agglomerates

Sample ID	Dilution from Stock Solution	Concentration (mg/mL)	Peak Diameter (nm)
5 (untagged)	---	0.92	2300,5500
A (untagged)	10 vol% in DI H_2O	0.050	615
B (untagged)	5 vol% in DI H_2O	0.025	250
C (untagged)	1 vol% in DI H_2O	0.005	530
4 (tagged)	---	0.54	615
D (tagged)	10 vol% in DI H_2O	0.054	105
E (tagged)	5 vol% in DI H_2O	0.027	105
F (tagged)	1 vol% in DI H_2O	0.005	140

Note: Samples A to F were created on 05-19-09 and analyzed on 05-20-09. Concentrations are approximately the same as those used in the MNP toxicity in HeLa cell studies.

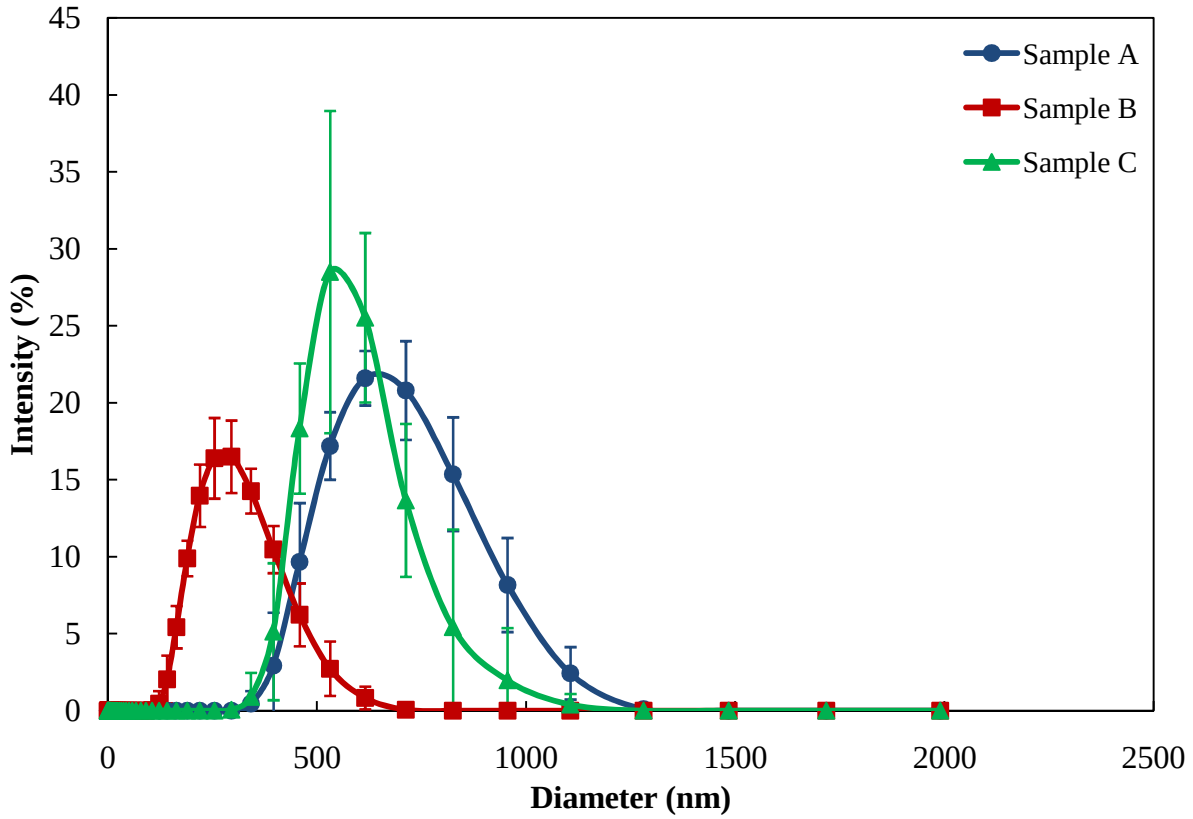

Figure 6.3 Comparison of Untagged $CoFe_2O_4$ Magnetic Nanoparticle Sizes for 1, 5, and 10 vol% Dilutions from Stock Solution. Actual Concentrations Found in Table 6.2. Error Bars Indicate Standard Deviation for Three Samples. Where Not Shown, Error Bars are Smaller Than the Data Symbols.

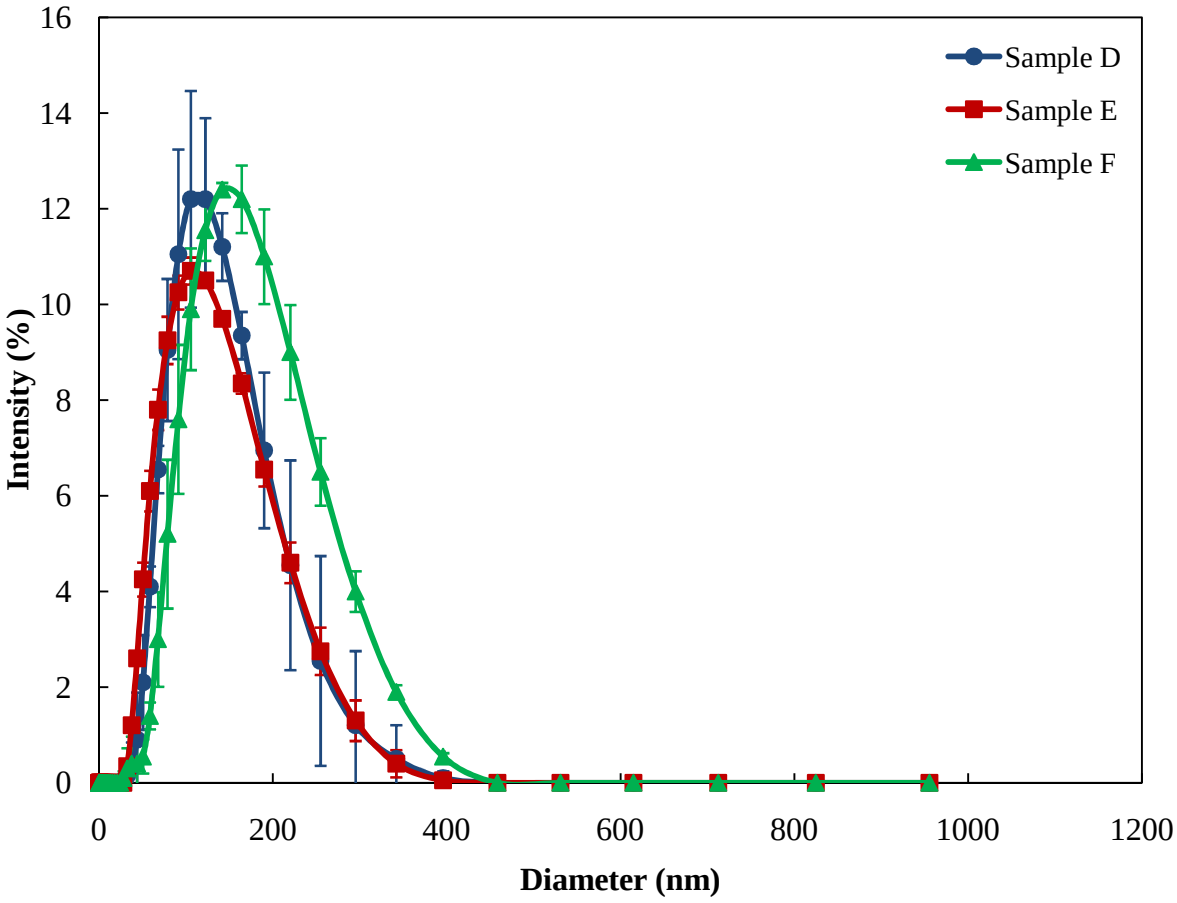

Figure 6.4 Comparison of Rhodamine-Tagged $CoFe_2O_4$ Magnetic Nanoparticle Sizes for 1, 5, and 10 vol% Dilutions from Stock Solution. Actual Concentrations Found in Table 6.2. Error Bars Indicate Standard Deviation for Three Samples. Where Not Shown, Error Bars are Smaller Than the Data Symbols.

Additionally, the results from this analysis show the same tendency for rhodamine-tagged $CoFe_2O_4$ nanoparticles to be smaller than untagged $CoFe_2O_4$. Figures 6.5, 6.6, and 6.7 present the data from Figures 6.3 and 6.4 to compare the sizes of rhodamine-tagged and untagged $CoFe_2O_4$ at approximately the same concentrations. The trend initially shown in Figure 6.1, that the addition of rhodamine dye to the surface of $CoFe_2O_4$ MNPs decreases average peak diameters, is seen at the three concentrations analyzed. The knowledge obtained in the DLS studies regarding the size of $CoFe_2O_4$ MNPs in solution and their stability will help us to understand and predict the mechanisms of MNP internalization in cells, as investigated in the following sections.

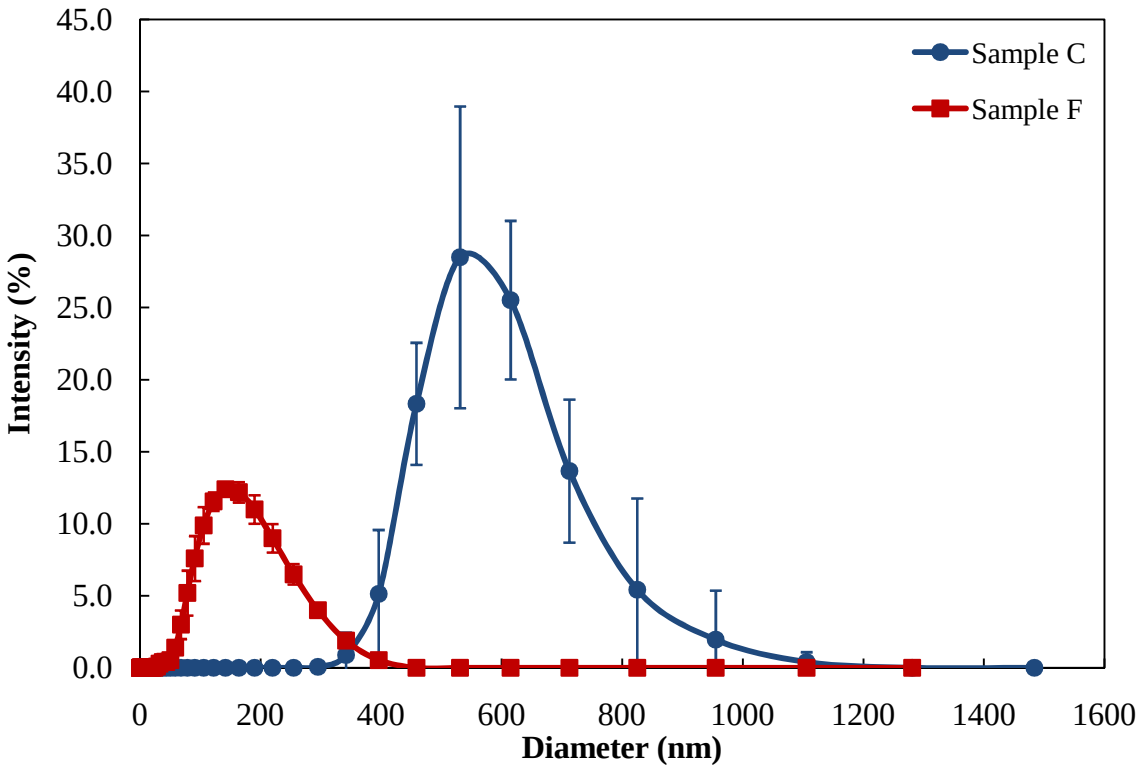

Figure 6.5 Comparison of Untagged and Rhodamine-Tagged $CoFe_2O_4$ Magnetic Nanoparticle Sizes Diluted to 1 vol% from Stock Solution. Actual Concentrations Found in Table 6.2. Error Bars Indicate Standard Deviation for Three Samples. Where Not Shown, Error Bars are Smaller Than the Data Symbols.

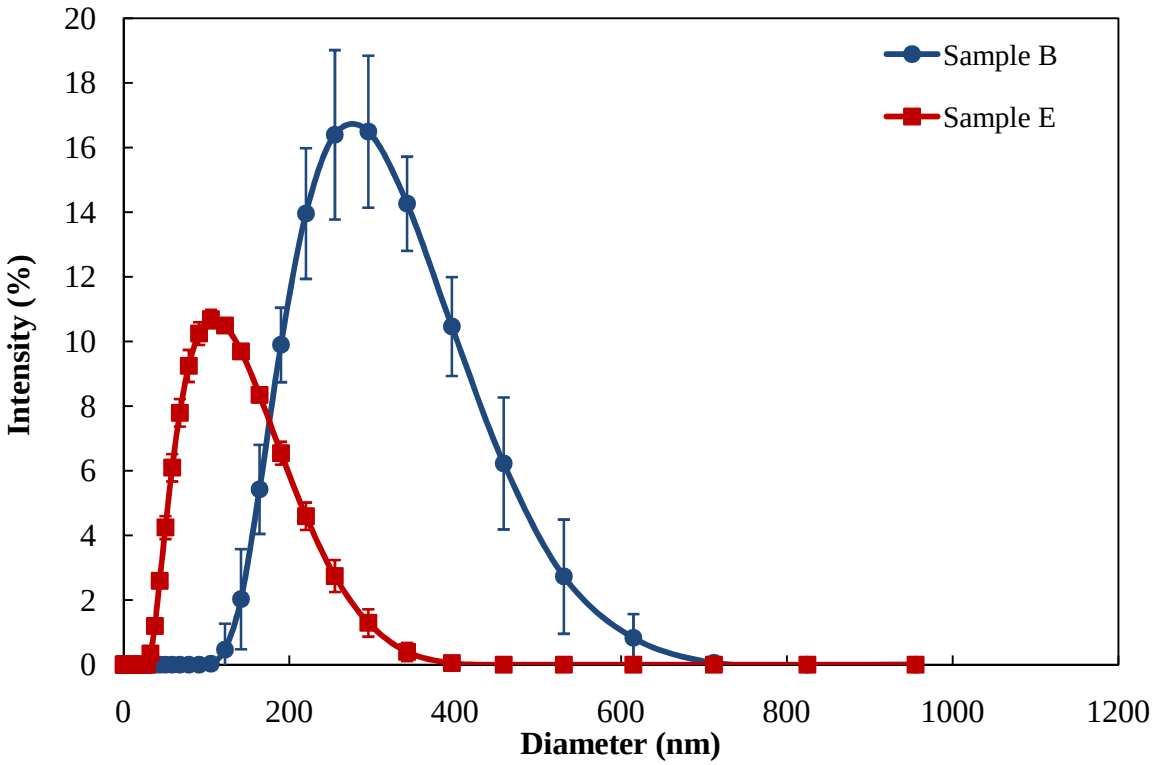

Figure 6.6 Comparison of Untagged and Rhodamine-Tagged $CoFe_2O_4$ Magnetic Nanoparticle Sizes Diluted to 5 vol% from Stock Solution. Actual Concentrations Found in Table 6.2. Error Bars Indicate Standard Deviation for Three Samples. Where Not Shown, Error Bars are Smaller Than the Data Symbols.

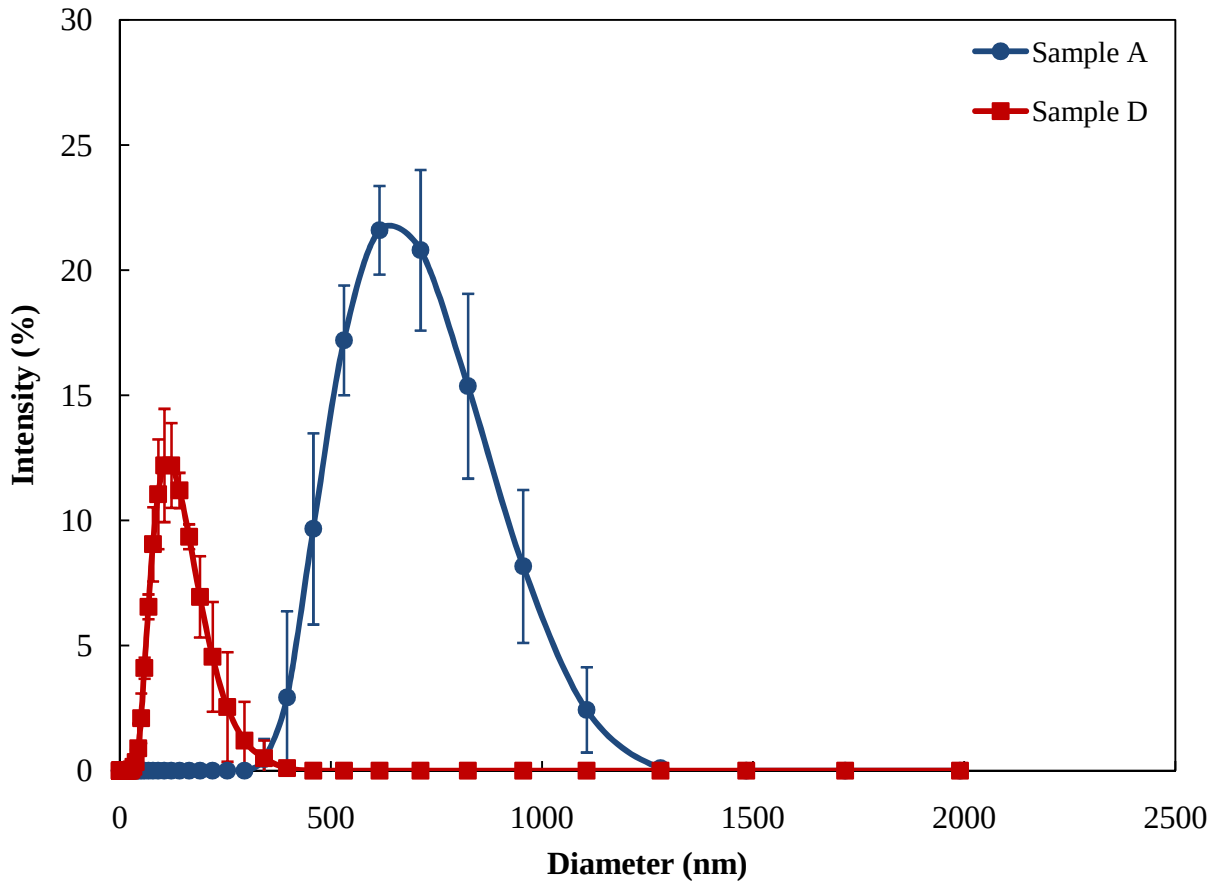

Figure 6.7 Comparison of Untagged and Rhodamine-Tagged $CoFe_2O_4$ Magnetic Nanoparticle Sizes Diluted to 10 vol% from Stock Solution. Actual Concentrations Found in Table 6.2. Error Bars Indicate Standard Deviation for Three Samples. Where Not Shown, Error Bars are Smaller Than the Data Symbols.

6.2 Toxicity of $CoFe_2O_4$ MNPs in HeLa Cells

Because the MNPs are being developed as a part of a therapeutic device to be applied *in vivo,* the cytotoxicity of MNPs to human cells was investigated as a function of concentration. The viability of HeLa cells exposed to $CoFe_2O_4$ MNPs was determined relative to the negative control (HeLa cells only) for varying concentrations of MNP solutions, including the concentration used in the internalization studies. Samples containing only MNP solutions were used as cell blank data, to account for the absorption of samples due to the colored MNP solutions. The average absorbance for the negative control containing no MNPs was set as the reference for relative viability. Equation 1 describes how relative viability was determined for each sample:

$$V = \frac{A_{ij} - B_{\%}}{\bar{A}_{Neg}} \tag{1}$$

where A_{ij} is the absorbance of the well on the i^{th} row (corresponding to different sample concentrations or descriptions) and j^{th} column (with measurements encompassing four replicates per sample type and concentration), $B_{\%}$ is absorbance of the cell blank for a specific % MNP solution, and $\bar{A}_{Neg}$ is the average absorbance of the negative control wells. The MNP solutions were diluted from a stock solution, with the actual concentrations of MNPs added to cell culture media being similar for the tagged and untagged MNPs (Table 6.4). Both rhodamine-tagged and untagged $CoFe_2O_4$ magnetic nanoparticles show little toxicity, with relative viability of the HeLa cells not statistically different from the negative (no MNP) control at dilutions up to 5% in media after 24 and 48 h of incubation, with some data reflecting a higher cell count with MNPs than the control, even (Figure 6.15 and 6.16). At or above a dilution of 7.5% , both rhodamine-tagged (0.0405 mg/mL) and untagged (0.0380 mg/mL) MNPs lead to decreased cell viability when the incubation time increases from 48 to 93 h, although the decrease in viability is not significant at

the 10% (~0.05 mg/mL) dilution. For most concentrations, the different periods of incubation did not show a significant effect on the relative viability of cells. Most samples showed greater viability than the positive control (H_2O_2) at all time points. The rhodamine-tagged and untagged MNPs at 7.5% (0.0405 mg/mL and 0.0380 mg/mL, respectively) in HeLa cells tested at 24 h showed no significant difference in toxicity levels than the positive control, indicating that the MNPs are causing cytoxicity at these levels or higher.

Table 6.3 Concentrations of Rhodamine-Tagged and Untagged $CoFe_2O_4$ MNPs used in Toxicity Studies

Rhodamine-Tagged $CoFe_2O_4$ MNPs	
Dilution of MNPs from Stock Solution (vol% in media)	**MNP Concentration in Media (mg/mL)**
1.0	0.0054
2.5	0.0135
5.0	0.0270
7.5	0.0405
10.0	0.0540
Untagged $CoFe_2O_4$ MNPs	
Dilution of MNPs from Stock Solution (vol% in media)	**MNP Concentration in Media (mg/mL)**
1.0	0.0051
2.5	0.0127
5.0	0.0253
7.5	0.0380
10.0	0.0506

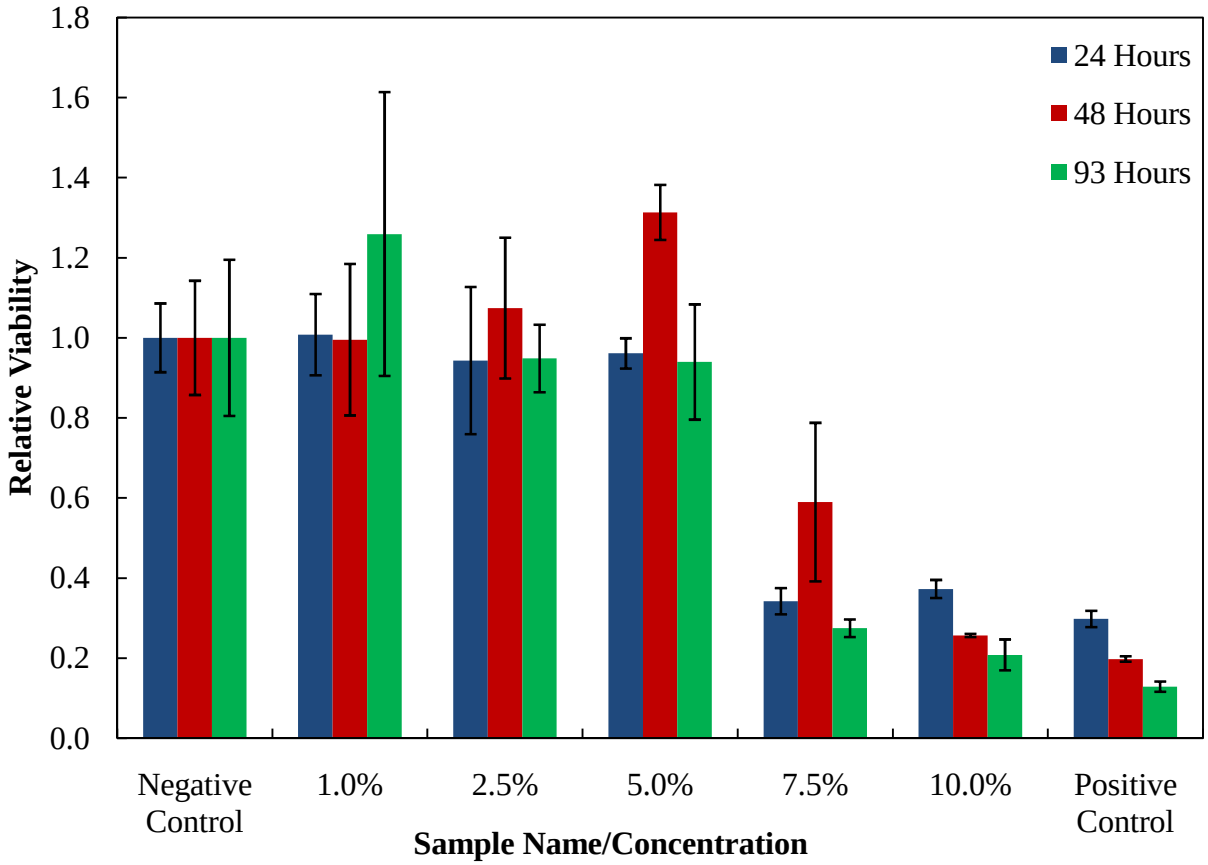

Figure 6.8 Relative Viability of HeLa Cells After Exposure to Various Concentrations of Rhodamine-Tagged $CoFe_2O_4$ Magnetic Nanoparticles over Time. Error Bars Indicate Standard Deviation for Four Samples.

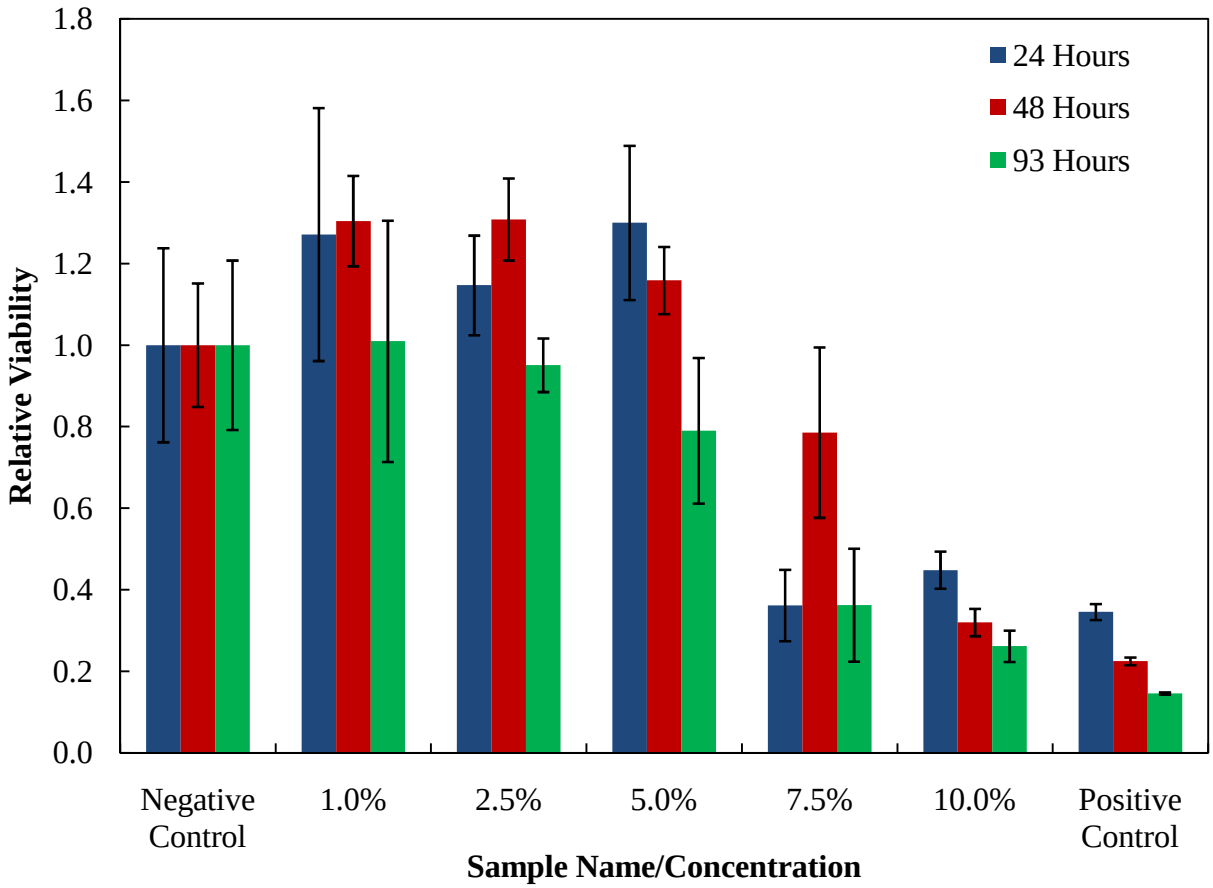

Figure 6.9 Relative Viability of HeLa Cells After Exposure to Various Concentrations of Untagged $CoFe_2O_4$ Magnetic Nanoparticles over Time. Error Bars Indicate Standard Deviation for Four Samples.

There was no significant difference seen between rhodamine-tagged and untagged MNPs at approximately the same concentrations after the same incubation period, as shown in Figures 6.17 and 6.18. These figures represent the data from Figures 6.15 and 6.16 to compare the relative viabilities of rhodamine-tagged and untagged $CoFe_2O_4$ MNPs in HeLa cells. For the samples that showed statistical differences in cell viability levels, the untagged $CoFe_2O_4$ MNPs lead to greater viability of HeLa cells than rhodamine-tagged MNPs at roughly the same concentration. The significant difference between rhodamine-tagged and untagged samples was the presence of rhodamine dye, attached via a thiol bond, to the surface of the MNPs. DMSA was present in both samples as the surfactant allowing for dispersion of the $CoFe_2O_4$ in water. Other studies have shown that DMSA has limited toxicity and good efficiency as a treatment for heavy metal poisoning [62, 63]. The reported LD_{50} for DMSA in mice is approximately 2000 mg/kg [63]. Rhodamine B has a reported LD_{50} value of 887 mg/kg in mice [64]. The toxicological behaviors observed in this study could be impacted by free DMSA or rhodamine that had broken away from the surface of the nanoparticles.

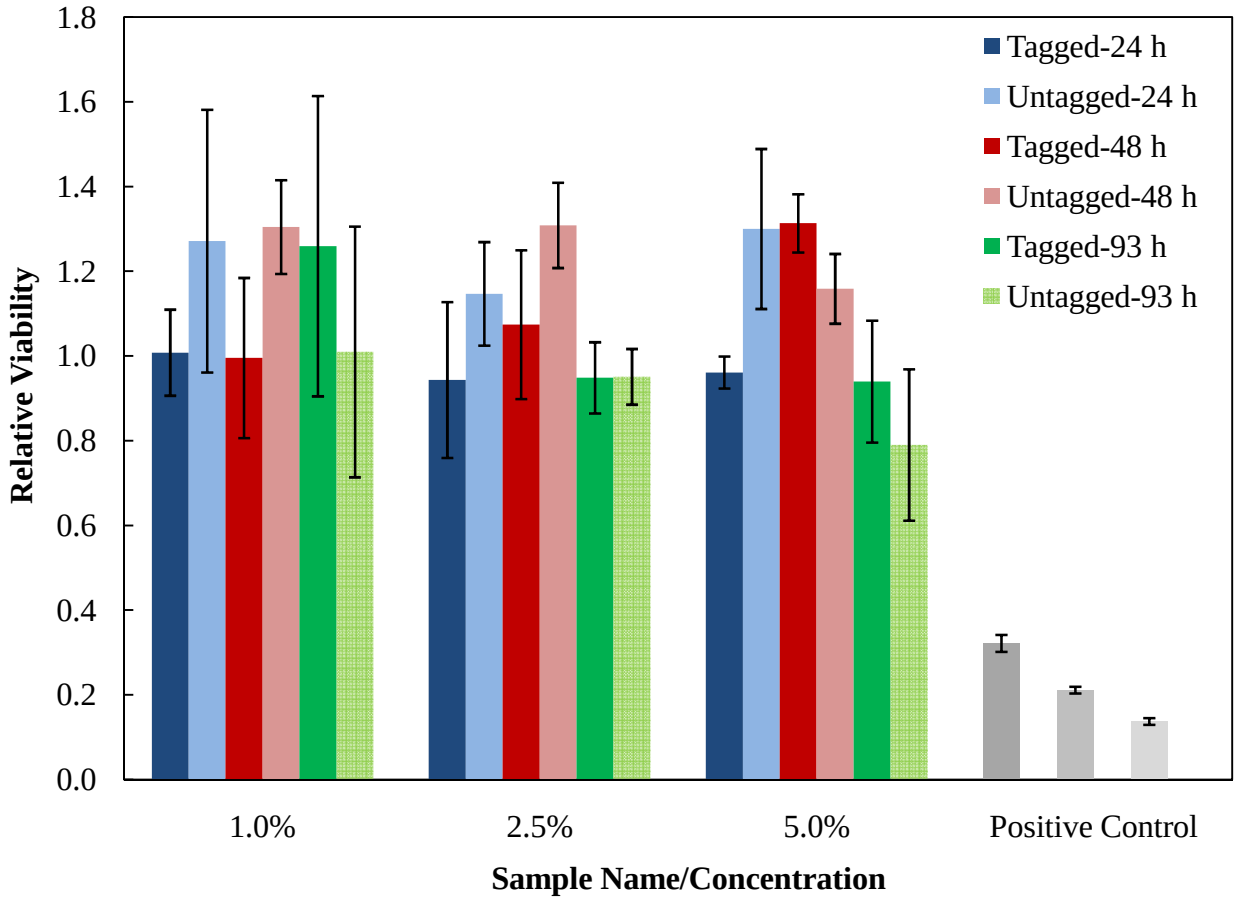

Figure 6.10 Relative Viability of HeLa Cells After Exposure to Low Concentrations of Rhodamine-Tagged and Untagged $CoFe_2O_4$ MNPs over Time. Compared with Relative Viability for Positive Control Cultures. Concentrations in mg/mL of Rhodamine-Tagged and Untagged $CoFe_2O_4$ MNPs are 0.0054 and 0.0051 (1.0%), 0.0135 and 0.0127 (2.5%), 0.0270 and 0.0252 (5.0%). Error Bars Indicate Standard Deviation for Four Samples.

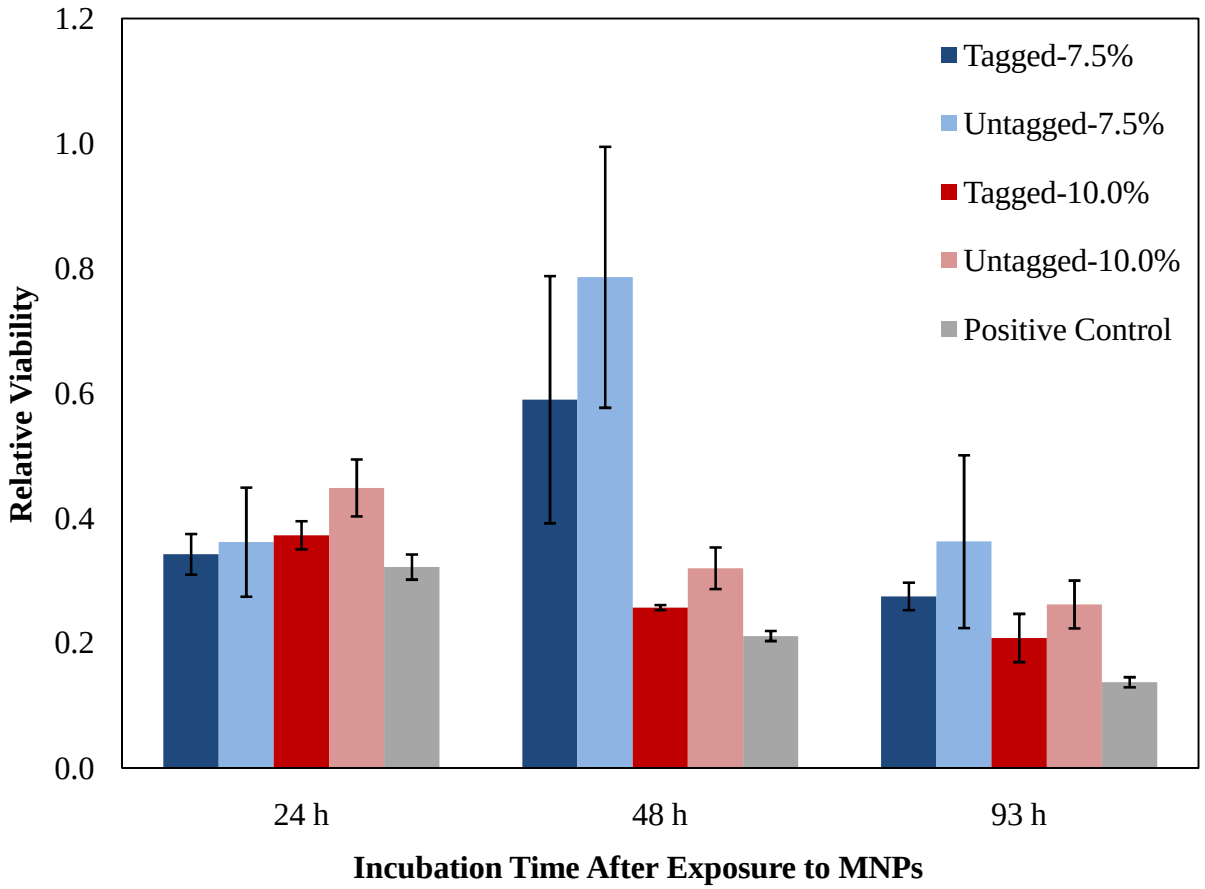

Figure 6.11 Relative Viability of HeLa Cells After Exposure to High Concentrations of Rhodamine-Tagged and Untagged $CoFe_2O_4$ MNPs over Time. Compared with Relative Viability for Positive Control Cultures. Concentrations in mg/mL of Rhodamine-Tagged and Untagged $CoFe_2O_4$ MNPs are 0.0405 and 0.0380 (7.5%) and 0.0540 and 0.0506 (10.0%). Error Bars Indicate Standard Deviation for Four Samples.

In most cases, concentrations of 7.5% or higher led to decreased cell viability. This suggests that the internalization of more MNPs has a negative effect on cells. This could be the result of an over accumulation of $CoFe_2O_4$ in the HeLa cells. Several previous studies with iron oxide MNPs have seen similar results. One of these studies showed that increasing the concentration of iron oxide MNPs exposed to rat neural cells from 0.15 mmol to 15 mmol led to a decrease in cell viability from 75% to less than 20% after 6 days exposure [61]. However, since $CoFe_2O_4$ does not biodegrade in the same manner as iron oxide MNPs, increased toxicity shown in these studies cannot be solely attributed to accumulation of iron in the cells. Further work needs to be done to determine if the $CoFe_2O_4$ MNPs are degrading *in vivo* and if this causes the increased toxicity. Other work has shown that fibroblast cell cultures exposed to $CoFe_2O_4$ showed greater than 85% viability at concentrations below 0.1mg/mL after 4 h incubation [33, 43]. As the concentration was increased above this point, the relative viability of the cells was shown to decrease. However, these particles were synthesized through a different method and did not contain the DMSA or rhodamine, which could account for the difference seen in safe concentrations of MNPs. In *in vivo* studies conducted by this same group, 1 mL of 10 mg/mL $CoFe_2O_4$ MNP solution was injected intravenously into mice weighing roughly 25 g, corresponding to a 400 mg/kg dosage [44]. The animals were monitored for seven weeks following the administration, and showed no clinical symptoms of toxicity and no significant weight change from the control group. Further work is needed to determine the mechanisms of cytoxicity of $CoFe_2O_4$ MNPs in cells and the maximum safe concentration to which cells can be exposed, for both short-term exposure as well as long-term effects, should it be shown that MNPs bioaccumulate in cells without being metabolized or removed.

6.3 Localization of Rhodamine-Tagged $CoFe_2O_4$ MNPs in HeLa Cells

In the 30 min incubation studies, HeLa cells were shown to take up both rhodamine-tagged and untagged $CoFe_2O_4$ MNPs. Table 6.3 gives the relative concentrations of MNP solutions included in the cell culture studies as well as the percentage of MNP solution in media. In Figure 6.12a, the HeLa cells under white light show regular morphology and good cell density. Under green light, no red fluorescence is seen in Figure 6.12b because no rhodamine-tagged $CoFe_2O_4$ MNPs are present. The cell membrane stain phalloidin could not be visualized at the time these images were collected due to a malfunctioning blue light in the Olympus fluorescence microscope. The 1% (0.0054 mg/mL) and 10% (0.054mg/mL) rhodamine-tagged MNPs in media samples showed normal cell morphology with some internalized MNPs (Figures 6.13a and 6.14a). In the cultures exposed to the untagged $CoFe_2O_4$ MNPs, the HeLa cells show altered morphology due to uptake of these particles (Figure 6.15a). When excited by 543 nm light, red fluorescence of the rhodamine-tagged MNPs can be seen (Figure 6.13b and 6.14b). In Figure 6.14b more of the red spots can be seen, which corresponds to the higher concentration of rhodamine-tagged $CoFe_2O_4$ to which the cells were exposed. A discussion of how these results were quantified is presented later in this section. Irregularly shaped cells indicate that the sample of 10% (0.506 mg/mL) untagged $CoFe_2O_4$ had a lower degree of biocompatibility than the corresponding rhodamine-tagged samples (Figure 6.15a). This could be caused by either the increased concentration of MNPs (which was about ten times more concentrated than the highest concentration of rhodamine-tagged MNP investigated), the size of the untagged MNPs, or the fact the MNPs were untagged. These studies have shown that the untagged MNPs led to irregular HeLa cell morphologies when added to cell cultures at high concentrations. For the localization study samples, the effective concentration of $CoFe_2O_4$ introduced to the HeLa cells

was approximately 0.5 mg/mL. In the toxicity studies, the greatest effective concentration of untagged MNPs introduced to the samples was roughly 0.05 mg/mL which led to a decrease in relative viability. These results support the suggestion that the higher concentration of untagged, compared to the lower concentration of rhodamine-tagged, $CoFe_2O_4$ MNPs in the localization studies led to decreased biocompatibility.

Table 6.4 Concentrations of Rhodamine-Tagged Magnetic Nanoparticles used in Localization Studies

Sample ID and Description	Dilution from Stock Solution	Concentration (mg/mL)	Incubation Time
HeLa cells- Low Concentration Rhodamine-Tagged MNPs	1% in media	0.006	30 min
HeLa cells- High Concentration Rhodamine-Tagged	10% in media	0.060	30 min
HeLa cells- Untagged MNPs	10% in media	0.51	30 min
HeLa cells- Rhodamine-Tagged	10% in media	0.054	2, 6, and 24 h

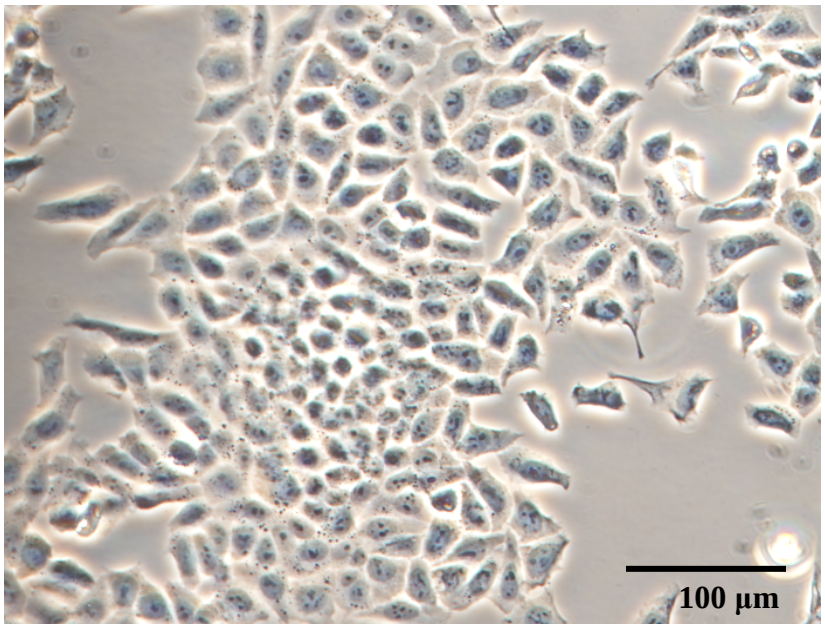

(a)

(b)

Figure 6.12 Fluorescence Microscope Images of Control Cells from HeLa Internalization of MNPs Studies under (a) White Light (b) Green Laser Stimulation. Because no Rhodamine-tagged MNPs are Present, Nothing Fluoresces in 6.12b. Scale Bars are Approximate. Representative Images Shown.

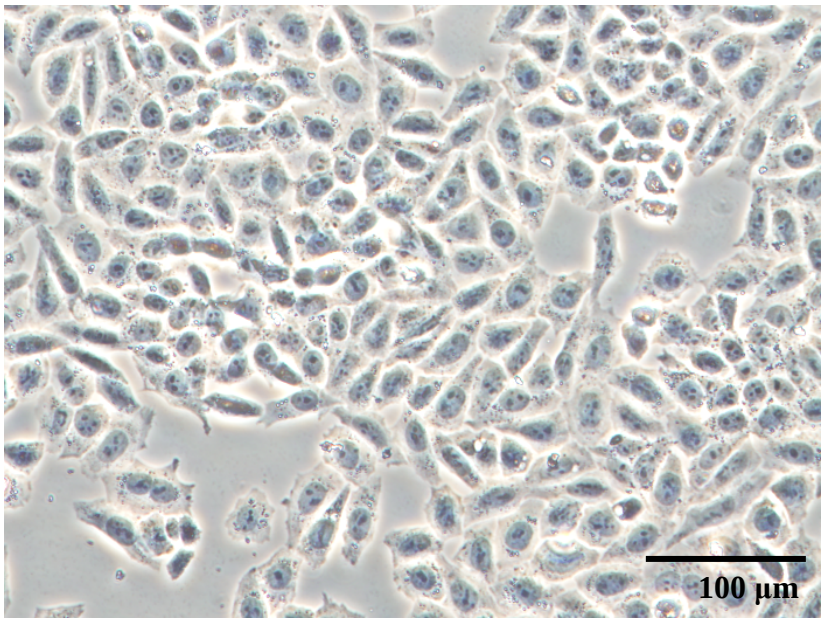

(a)

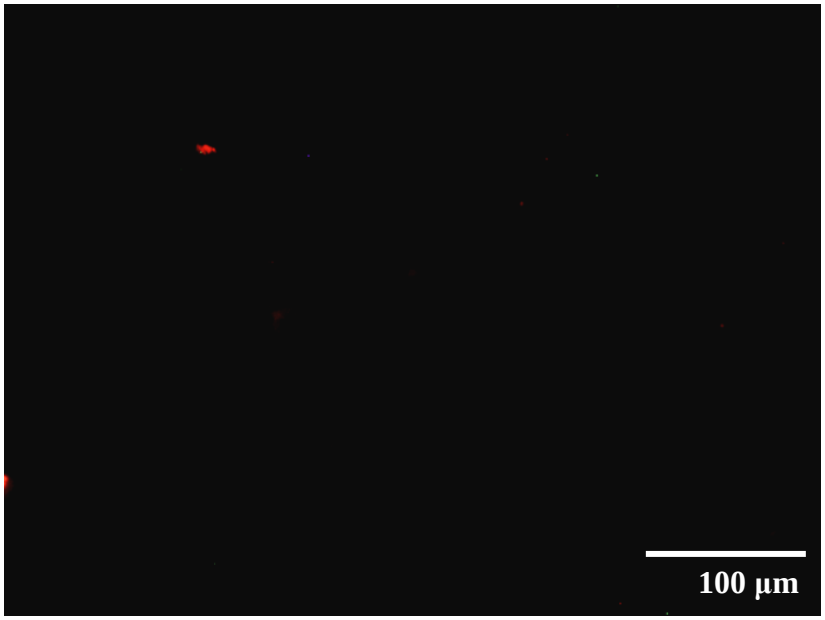

(b)

Figure 6.13 Fluorescence Microscope Image of HeLa Cells Fed 1 vol% (0.006 mg/mL) Rhodamine-Tagged $CoFe_2O_4$ in Media and Incubated for 30 min under (a) White Light (b) Green Laser Stimulation. Scale Bars are Approximate. Representative Images Shown.

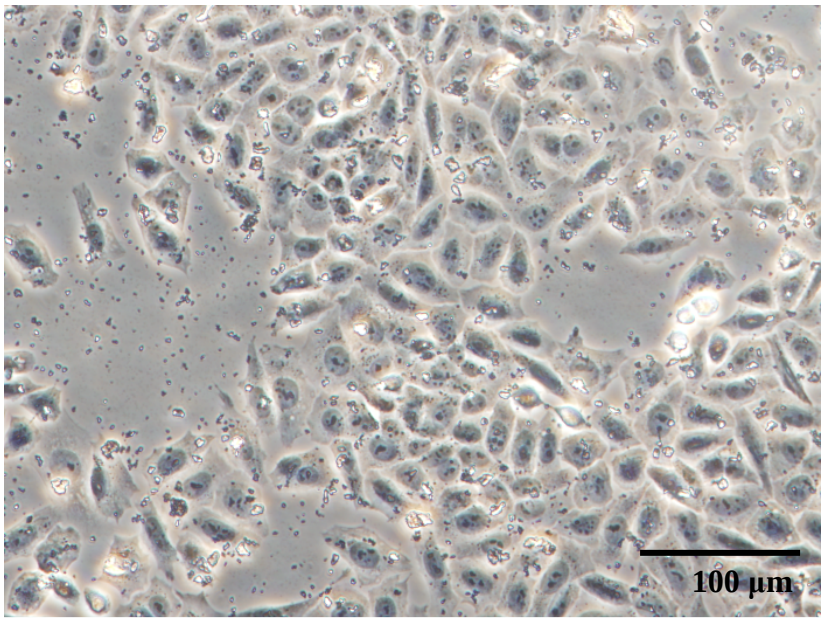

(a)

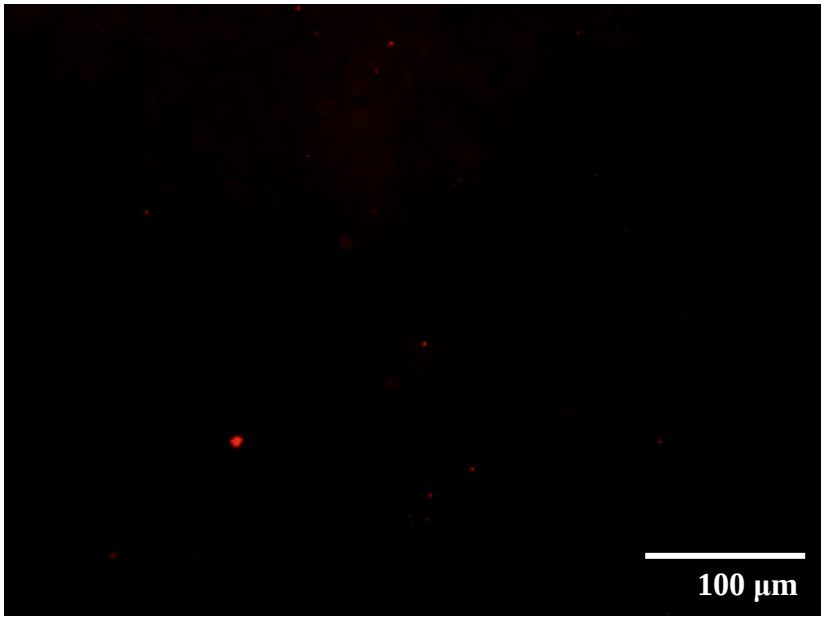

(b)

Figure 6.14 Fluorescence Microscope Image of HeLa Cells Fed 10 vol% (0.06 mg/mL) Rhodamine-Tagged $CoFe_2O_4$ in Media and Incubated for 30 min under (a) White Light (b) Green Laser Stimulation. Scale Bars are Approximate. Representative Images Shown.

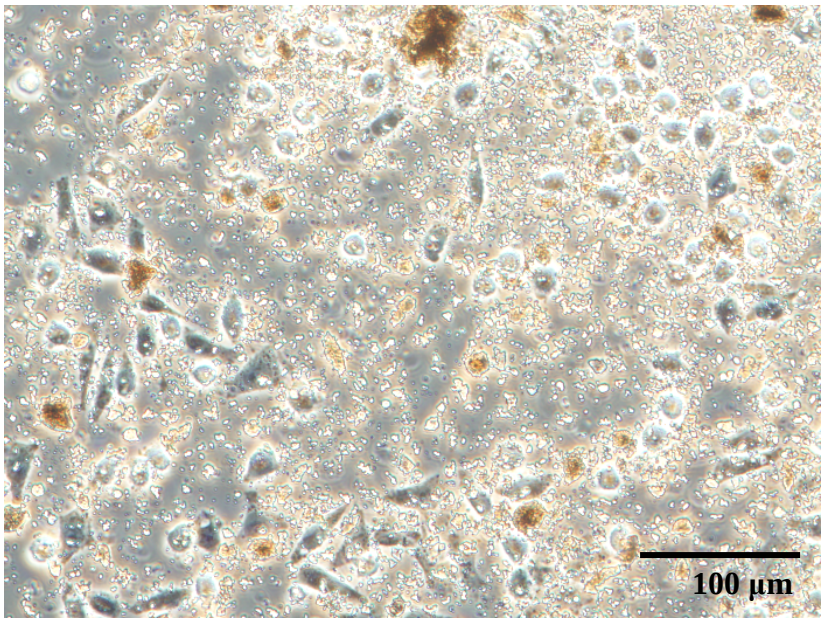

(a)

(b)

Figure 6.15 Fluorescence Microscope Images of HeLa Cells Fed 10 vol% (0.506 mg/mL) Untagged $CoFe_2O_4$ in Media and Incubated for 30 min under (a) White Light (b) Green Laser Stimulation. Because the $CoFe_2O_4$ MNPs did not have the Rhodamine tag, They do not Fluoresce in 6.15b. Scale Bars are Approximate. Representative Images Shown.

The internalization of rhodamine-tagged $CoFe_2O_4$ MNPs was investigated as a function of incubation time. A partition coefficient was defined and determined for confocal microscope images of the HeLa cells after different exposure times to the MNPs. The coefficient allows for a quantitative comparison regarding the uptake of rhodamine-tagged MNPs as a function of time. The definition of K and procedure for determining it are described below. As the incubation time increased from 30 min to 2 and 6 h, HeLa cells exposed to 10% (0.054 mg/mL) rhodamine-tagged $CoFe_2O_4$ MNPs showed regular cell morphology and good cell density, as well as uptake of the MNPs (Figure 6.16c and Figure 6.17a). The phalloidin-stained cell membranes allowed for visualization of whether MNPs had been internalized into the cells (Figure 6.16a). At 2 h incubation time, red fluorescence is seen inside the cells while some aggregates remain outside of the cells (Figure 6.16b and c). Intense red fluorescence seen in Figures 6.16c, 6.17a, and 6.17b correspond to aggregates of rhodamine-tagged $CoFe_2O_4$ MNPs. After 24 h the HeLa cells have a slightly less regular morphology, indicating a lower degree of biocompatibility of the MNPs after prolonged periods of exposure (Figure 6.17b).

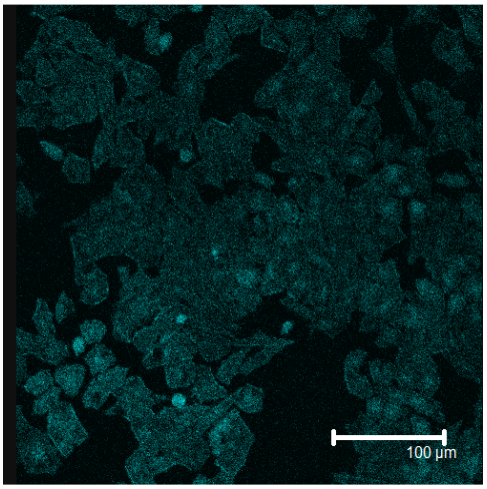

(a)

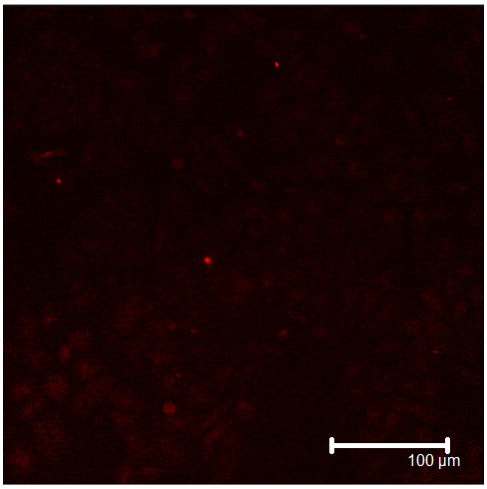

(b)

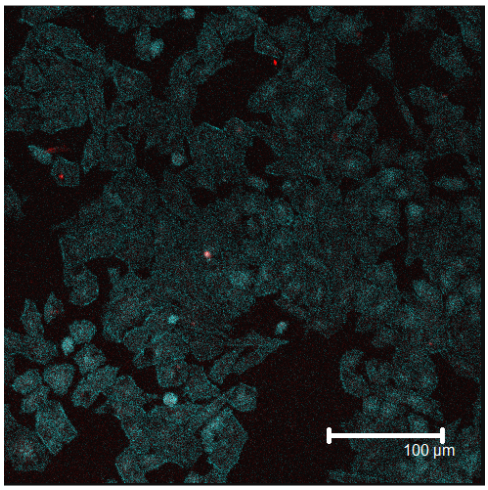

(c)

Figure 6.16 Confocal Microscope Images of HeLa Cells at 20X Magnification After 2 h Exposure to 10 vol% (0.054 mg/mL) Rhodamine-Tagged $CoFe_2O_4$ MNPs Under (a) Green Filter (b) Red Filter and (c) Overlay of Green and Red Filters. The Scale is 100 µm. Note: The Green Filter is Shown with Cyan False Coloring, Due to a Glitch in the Leica Microscope Software. Representative Images Shown.

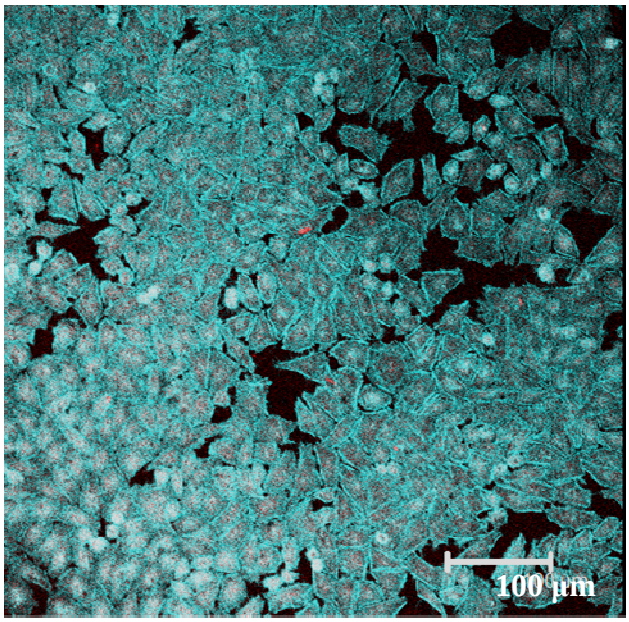

(a)

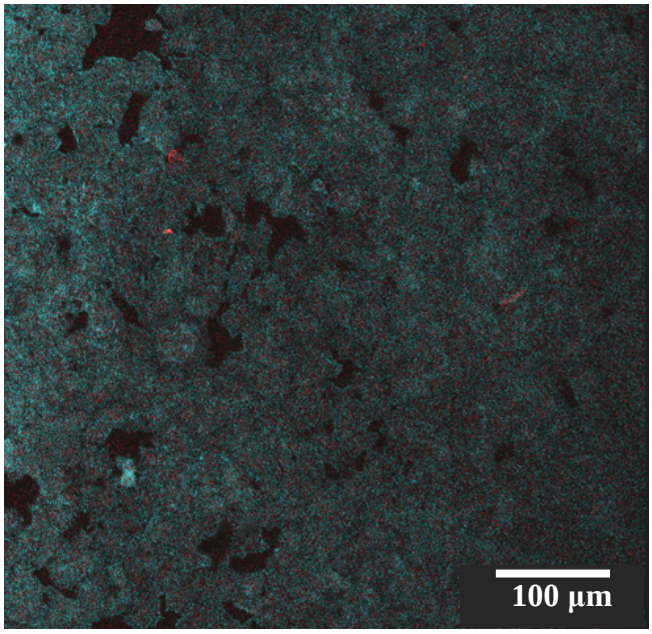

(b)

Figure 6.17 Confocal Microscope Images of HeLa Cells at 20X Magnification and Exposure to 10 vol% (0.054 mg/mL) Rhodamine-Tagged $CoFe_2O_4$ MNPs. Incubation Times were (a) 6 h and (b) 24 h. The Images Represent Overlays of the Green and Red Channels. Note: The Green Channel is Shown with Cyan False Coloring, Due to a Glitch in the Leica Microscope Software. Representative Images Shown.

To quantify and compare internalization of rhodamine-tagged $CoFe_2O_4$ MNPs in HeLa cells, analysis using ImageJ software was completed on confocal microscope images of the cells taken after 30 min, 2, 6, and 24 hours post-incubation with 10vol% rhodamine-tagged $CoFe_2O_4$ MNPs [65]. Any red fluorescence inside cells was considered internalized MNPs. This analysis interpreted any MNPs localized to the cell membrane as internalized. From ImageJ, the areas of red fluorescence inside and outside cells in a specific image were measured. In the same image, the total area of cells and intracellular spaces were measured. The results were reported as partition coefficients K. Three representative images for each time point were analyzed in this manner and the results are given in Figure 6.14. The figures used in this analysis are included in Appendix 3. The equation used to calculate K is given below:

$$K = \frac{A_{RC} / A_C}{A_{RO} / A_O} \tag{2}$$

where A_{RC} is the area of red fluorescence inside the cells, A_C is the area of the cells, A_{RO} is the area of red fluorescence outside the cells, and A_O is the area outside (intracellular) the cells in the image. A K value below one represents the tendency for the nanoparticles to remain outside the cells, while a K value greater than one indicates the preference for the cells to internalize MNPs. When K is one, the concentrations of MNPs inside and outside the cells are equal.

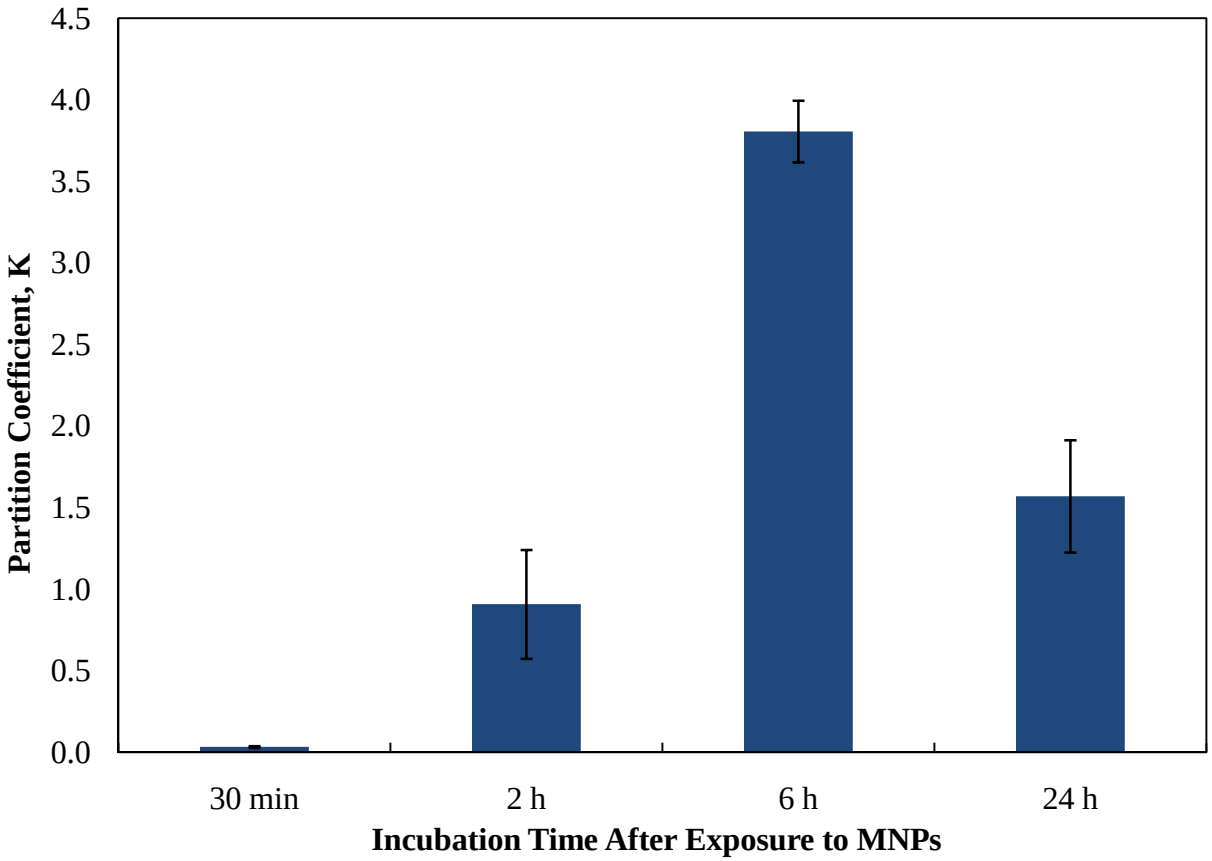

Figure 6.18 Partition Coefficients K for Rhodamine-Tagged $CoFe_2O_4$ Magnetic Nanoparticles in HeLa Cells over Time. Error Bars Indicate Standard Deviation for Three Analyzed Representative Images.

Partitioning of 10 vol% rhodamine-tagged $CoFe_2O_4$ MNPs in HeLa cells was studied as a function of incubation time (Figure 6.14). An increase in K of rhodamine-tagged $CoFe_2O_4$ in HeLa cells can be seen as the incubation time increases from 0.033 at 30 min to 3.805 at 6 hours. Because the K value after 30 min incubation is much smaller than 1, initially few MNPs were internalized and the concentration of rhodamine-tagged MNPs outside the cell remained dominant. After 2 h of incubation, the concentrations of MNPs inside and outside the cells were nearly equal with K = 0.907. The partition coefficient at 6 h was four times K at 2 h, indicating internalization of rhodamine-tagged MNPs far greater than what could be achieved through passive diffusion. Because the K value at 6 h is much greater than 1, the concentration of rhodamine-tagged MNPs inside the cells is dominant compared to the concentration outside the cells. The increase in the partition coefficient of tagged MNPs over time suggests an active uptake process by the cells, such as endocytosis. At 24 h, there is a decrease in the ratio of MNPs inside the cells to outside the cells. The decrease in internalized MNPs is a result of the cytoxicity of the rhodamine-tagged $CoFe_2O_4$ solution, which causes cell membranes to burst, spilling previously internalized MNPs into the growth media outside the cells, although the remaining living cells still had an affinity for the MNPs (K > 1). Results from toxicity screenings indicate that at 24 h, the 10 vol% (0.054 mg/mL) rhodamine-tagged MNP concentration used to study internalization is toxic to HeLa cells. In the images, these released MNPs appear in the red fluorescence outside cells. The result is a decrease in the observed internalization as denoted by K.

The results from the internalization and localization studies of rhodamine-tagged MNPs into HeLa cells show the cells readily internalize the MNPs, but result in cell death at the concentrations studied. Further experiments are needed to determine if the particles released

from the apoptotic cells can be internalized by viable cells. This could occur through phagocytosis if the viable cell internalizes cell debris containing the MNPs. The time dependence and K values greater than one seen in the internalization studies support an active process such as endocytosis as the mechanism for MNP uptake. These findings agree with other projects that report endocytosis as the most likely mechanism by which MNPs are internalized in different cell lines [53, 66]. Other studies indicate a time dependent process such as endocytosis by showing quick uptake of iron oxide MNPs in HeLa cells at incubation times below 5 hours and a leveling off effect as incubation time increases up to 10 hours [53]. Further localization studies, with the inclusion of multiple stains for better colocalization analysis, should be used to help determine the mechanism responsible for MNP internalization.

6.4 Toxicity Studies of Rhodamine-Tagged $CoFe_2O_4$ MNPs in *C. Elegans* Worms

Previously mentioned work discusses how the MNPs behave in human cell cultures, but at the organism level the different types of tissue and distribution mechanisms may impact how the MNPs are internalized and tolerated. Wild type and mutant *C. elegans* worms exposed to rhodamine-tagged $CoFe_2O_4$ MNPs were capable of reproducing. For all exposure times, the MNP solution showed no visible effects on worm health and reproduction. In initial studies, an older sample of rhodamine-tagged $CoFe_2O_4$ MNPs fed to the worms killed wild type specimens immediately upon exposure, but it is difficult to draw conclusions because the exact age and concentration of that MNP solution is unknown. A thorough quantitative toxicity screening is required before the rhodamine-tagged $CoFe_2O_4$ MNPs can be conclusively declared non-toxic. Confocal laser scanning microscopy was used to visualize worms from these studies, but due to complications with bleed over and autofluorescence, conclusive evidence of colocalization could not be determined. For a discussion of these experiments, see Appendix 4.

Chapter 7

CONCLUSIONS

The behavior of rhodamine-tagged $CoFe_2O_4$ magnetic nanoparticles in biological systems was studied to determine the suitability of the particle for inclusion in a cancer treatment platform. MNPs were synthesized and tagged with a fluorescent dye before being exposed to HeLa cells. The toxicological properties of these nanoparticles were investigated in HeLa cells and *C. elegans* worms. The localization of the particles was studied in the HeLa cells. Based on results obtained from this project, the use of these MNPs in combination cancer therapy platforms is feasible, though further work is needed in optimizing the biological properties of the materials.

The MNPs synthesized in the project showed a large range of sizes when placed in solution, depending on concentration and solvent used and whether rhodamine dye was attached to the surface. Agglomerations with greater than 1 μm diameters were seen in concentrated and older MNP solutions. Rhodamine was successfully attached to the surface of the $CoFe_2O_4$ MNPs. The addition of the fluorescent dye added to the stability of the MNP solution and decreased the average size of MNPs in solution. At approximately the same concentrations as untagged samples, the average peak diameter was reduced from 1280 nm to 615 nm for rhodamine-tagged MNPs in aqueous solution. When diluted to concentrations of approximately 0.05 mg/mL, there was a significant decrease in the average size of the particle, with rhodamine-tagged $CoFe_2O_4$ MNPs showing average peak diameters around 100 nm.

The localization of rhodamine-tagged $CoFe_2O_4$ magnetic nanoparticles was investigated in HeLa cells. In the HeLa cell studies, the fluorescent MNPs were internalized into the cytoplasm of cells. The relative amount of $CoFe_2O_4$ MNPs internalized, as measured by K, increased as time increased, up until 6 h incubation time. At 24 h incubation time, the cytotoxic properties of the nanoparticles lowered the number of viable cells and thus the amount of MNPs internalized.

A toxicity screening of the rhodamine-tagged and untagged $CoFe_2O_4$ MNPs was performed using HeLa cells and *C. elegans* worms. The results from HeLa cell studies indicate that both sets of MNPs are safe at levels roughly 0.025 mg/mL in media or below. In most cases, samples of $CoFe_2O_4$ MNPs showed less toxicity than the positive control samples. There was no significant difference in concentrations from 0.005 mg/mL to 0.025 mg/mL, and time periods up to 93 h between rhodamine-tagged and untagged $CoFe_2O_4$ MNPs. When a difference was seen, the untagged particles were less toxic to the cells. In the *C. elegans* worms, the rhodamine-tagged MNPs did not affect the reproductive abilities of the wild type and mutant worms. Additional work is needed to better characterize the toxicological properties of $CoFe_2O_4$ for medical applications, including bioaccumulation behaviors and the potential for long-term toxicological effects.

Major conclusions for the study of localization and behavior of rhodamine-tagged magnetic nanoparticles in biological systems are listed below:

A. Rhodamine-tagged $CoFe_2O_4$ magnetic nanoparticle solutions have average diameters near 100 nm when diluted to 0.05 mg/mL.
B. Rhodamine-tagged $CoFe_2O_4$ magnetic nanoparticles are taken up in a time-dependent manner into HeLa cells as incubation time increases from 30 min to 6 h.

C. Both rhodamine-tagged and untagged $CoFe_2O_4$ magnetic nanoparticles show no effect on relative viability of HeLa cells at or below concentrations of roughly 0.025 mg/mL up to 93 h after exposure.

Chapter 8

RECOMMENDATIONS

The purpose of this project was to investigate the behavior of $CoFe_2O_4$ magnetic nanoparticles in living systems. The MNPs are a portion of a novel combination cancer treatment platform that integrates hyperthermia and chemotherapy. For use in the therapy platform, it was necessary to study the toxicological properties of the $CoFe_2O_4$ MNPs. Although limiting the concentration of MNPs showed greater solution stability and more biologically suitable particle diameters, magnetic properties such as saturation magnetization and specific absorption ratios still need to be retained for use in hyperthermia therapy. To better formulate the overall design of the multifunctional platform, additional work is needed to ensure monodisperse MNPs of an appropriate size for medical applications. The MNPs must be monodisperse to ensure efficient heating in hyperthermia and still be small enough for cell membrane interactions *in vivo*.

Additional work to characterize the $CoFe_2O_4$ MNPs should include electron microscopy to help verify the sizes of the particles as determined by DLS. Techniques such as cryogenic transmission electron microscopy (TEM) would aid in studying the size distribution of MNPs in culture media. Thermo-gravimetric analysis on rhodamine-tagged and untagged $CoFe_2O_4$ magnetic nanoparticles could help determine relative amounts of DMSA and rhodamine attached to the surface of MNPs. Energy-dispersive X-ray spectroscopy (EDX) could be used to verify the composition of the nanoparticles. This technique could also be used to analyze

cells exposed to the magnetic nanoparticles to verify that the $CoFe_2O_4$ enters the cells. By coupling EDX with scanning electron microscopy, it would be possible to observe cobalt and iron localization with rhodamine fluorescence from tagged MNPs. To verify the surface chemistry related to the rhodamine-tagged MNPs, infrared spectroscopy could be used. Another recommended study includes using DLS to determine the size of rhodamine-tagged and untagged MNPs as a function of time. The procedures discussed represent methods to characterize the physical properties of the MNPs in solutions that mimic *in vivo* conditions. An understanding of these properties is important in the design of the nanoparticles if they are to be incorporated in a cancer treatment platform.

The fluorescent rhodamine tag on the MNP surface allowed for localization studies in biological systems. Rhodamine B was chosen as the fluorophore because the reaction chemistry to attach the dye to MNPs dispersed in water with DMSA was well-characterized. However, a thorough understanding of the behavior of the fluorescent tag on the MNPs at physiological conditions is still needed. Because the rhodamine is attached to the $CoFe_2O_4$ via a thiol bond, this represents a possible location for competing ligands and protein interactions in biological systems. Future studies should be completed to determine whether or not the rhodamine remains attached to the MNP in these conditions. Another possible study could utilize a different fluorophore attached to the surface of the magnetic nanoparticles. Changing the fluorescent dye tagged to $CoFe_2O_4$ MNPs could affect the behaviors and properties previously discussed such as hydrodynamic diameter. These particles may also present different uptake and localization behavior in biological systems.

In the localization studies for HeLa cells, the results indicate uptake of $CoFe_2O_4$ MNPs. A more thorough analysis of localization in the HeLa cells is needed to determine exactly where

the MNPs localize. One recommendation for future studies is diluting the cells before fixing and imaging. By decreasing the cell density on a slide before analysis, clearer images can be obtained. An additional suggestion is to expose the cells to a smaller concentration of MNPs before analysis with the confocal microscope. Limiting the concentration studied will show more precisely where the MNPs accumulate, as a sufficiently high concentration of rhodamine-tagged $CoFe_2O_4$ can overwhelm the confocal microscope and appear as a red haze throughout the cells in the collected images. Three-dimensional images, or z-stacks, would also be useful to determine that the MNPs have internalized and more precisely where they are located within a cell when used in combination with stains for different organelles and a more specific stain for the lipid bilayer than phalloidin. Continued work in this area will include the addition of targeting moieties on the surfaces of the MNPs to direct the particles to specific cell types, such as cancer cells. These particles can be visualized using the rhodamine-tagged MNPs developed in this project. Another suggestion for better analysis is to use more efficient membrane and internal membrane stains. The phalloidin used to visualize cell membranes stains actin filaments associated with the cell's membrane. While the membranes can be visualized this way, it does not provide a sharp enough contrast between the external and internal environment to be analyzed with ImageJ software. The internal membrane stains will allow the visualization of membrane-bound organelles within the cell, which will show better detail of localization of MNPs within the cell. Another suggested study includes conducting a mass balance to determine the MNPs remaining in media after the incubation periods. This data could be used to determine the percent uptake of MNPs in HeLa cells.

While most rhodamine-tagged $CoFe_2O_4$ MNPs appeared to remain in the GI tract of *C. elegans* worms, some images suggested colocalization of MNPs in the neurons. Because of the

technical problems of autofluorescence and bleed over, the results of the localization studies in wild type and mutant *C. elegans* worms are not conclusive enough to determine the behavior of the MNPs *in vivo.* A better understanding of these properties in a group of control *C. elegans,* which are not exposed to the rhodamine-tagged MNPs, is required. A discussion of the recommended protocol for these experiments is included in Appendix 5. A suggestion for a future study with *C. elegans* and MNPs is to try targeted MNPs or manganese-based materials. Current research indicates that manganese nanoparticles have a tendency to localize in neural tissues [67]. Studying the localization of targeted nanoparticles in *C. elegans* might show how the particles are absorbed through the lumen and accumulate in other tissues.

In addition to future localization studies, further investigation of the toxicological properties is needed before the MNPs are ready for use in a medical application. Toxicity screenings in the model organism *C. elegans* showed the rhodamine-tagged MNPs did not significantly affect the ability of the worms to reproduce. These studies were not sufficient to conclusively determine toxicological properties of the MNPs at the whole organism level. By changing any parameter of the MNP sample, such as size, concentration, or the addition of targeting or imaging moieties, the toxicological properties of the MNPs also change. These studies would also be suitable for determining the mechanisms of cytotoxicity and localization of MNPs *in vivo*.

Another recommended study derived from this project would be the investigation of localization and toxicity behavior of fluorescently-tagged magnetic nanoparticles in herpes simplex virus (HSV). This provides a potential vector for combination gene therapy and hyperthermia treatment. The HSVs can be genetically engineered with no infectivity and ability to reproduce *in vivo*. When functionalized MNPs with targeting moieties and imaging agents are

internalized into HSVs, the viruses become ideal agents for attacking individual cancer cells useful for diagnostic and therapeutic purposes. The therapeutic portion of the vector is two-fold: if the magnetic hyperthermia does not kill the cancer cell, the gene therapy aspect will be able to treat the patient. In these studies, toxicity and localization experiments would also need to be performed. Results would help determine how to incorporate the multi-functionalized nanoparticles into the viruses.

REFERENCES

1. Gao, J. and B. Xu. "Applications of nanomaterials inside cells," *nanotoday*, **4** (2009) 37-51.

2. Shubayev, V. I., T. R. Pisanic II, and S. Jin. "Magnetic nanoparticles for theragnostics," *Advanced Drug Delivery Reviews*, **61** (2009) 467-477.

3. Gupta, A. K., and A. S. Curtis. "Surface modified superparamagnetic nanoparticles for drug delivery: Interaction studies with human fibroblasts in culture," *Journal of Material Sciences*, **15** (2004) 493-496.

4. Corot, C., P. Robert, J.-M. Idée, and M. Port. "Recent advances in iron oxide nanocrystal technology for medical imaging," *Advanced Drug Delivery Reviews*, **58** (2006) 1471-1504.

5. "Cancer Statistics," National Cancer Institute, United States of America, <http://www.cancer.gov/statistics>.

6. "What is Cancer?" National Cancer Institute, United States of America, <http://www.cancer.gov/cancertopics/what-is-cancer>.

7. 1950 Mortality Data - CDC/NCHS, NVSS, Mortality Revised. 2004 Mortality Data: US Mortality Public Use Data Tape, 2004, NCHS, Centers for Disease Control and Prevention, 2006.

8. NCI Alliance for Nanotechnology in Cancer, National Cancer Institute, United States of America, <http://www.nano.cancer.gov>.

9. "Types of Treatment," National Cancer Institute, United States of America, < http://www.cancer.gov/cancertopics/treatment/types-of-treatment >.

10. Frei, E. "Combination Cancer Therapy: Presidential Address," *Cancer Research*, **32** (1972) 2593-2607.

11. Herskovic, A., K. Martz, M. al-Sharraf, L. Leichman, J. Brindle, V. Vaitkevicius, J. Cooper, R Byhardt, L. Davis, and B. Emami. "Combined chemotherapy and radiotherapy compared with radiotherapy alone in patients with cancer of the esophagus," *The New England Journal of Medicine*, **326** (1992) 1593-1598.

12. Brazel, C. S. “Magnetothermally-responsive Nanomaterials: Combining Magnetic Nanostructures and Thermally-Sensitive Polymers for Triggered Drug Release,” *Pharmaceutical Research*, **26** (2009) 644-656.

13. Kim, D.-H., S. Lee, K.-N. Kim, K.-M. Kim, I. Shim, and Y. Lee. “Temperature changes of various ferrite particles with alternating magnetic field for hyperthermic application,” *Journal of Magnetism and Magnetic Particles*, **293** (2005) 320-327.

14. Dobson, J. “Magnetic Nanoparticles for Drug Delivery,” *Drug Development Research*, **67** (2006) 55-60.

15. Gupta, A. K. and M. Gupta. “Synthesis and surface engineering of iron oxide nanoparticles for biomedical applications,” *Biomaterials*, **26** (2005) 3995-4021.

16. Nielsen, O.S., M. Horsman, and J. Overgaard. “A future for hyperthermia in cancer treatment?” *European Journal of Cancer*, **37** (2001) 1587-1589.

17. Shinkai, M. “Functional magnetic particles for medical application,” *Journal of Bioscience and Bioengineering*, **94** (2002) 606-613.

18. Jordan, A., R. Scholz, P. Wust, H. Fähling, J. Krause, W. Wlodarczyk, B. Sander, Th. Vogl, and R. Felix. “Effects of Magnetic Fluid Hyperthermia (MFH) on C3H mammary carcinoma *in vivo*,” *International Journal of Hyperthermia*, **13** (1997) 587-605.

19. Habib, A. H., C. L. Ondeck, P. Chaudhary, M. R. Bockstaller, and M. E. McHenry. “Evaluation of iron-cobalt/ferrite core-shell nanoparticles for cancer therapy,” *Journal of Applied Physics*, **103** (2008) 103-105.

20. Corot, C., K. G. Perry, R. Trivedi, A. Saleh, C. Jonkmanns, J. Le Bas, E. Bleezer, M. Rausch, B. Brochet, P. Foster-Gareau, D. Balèriaux, S. Gaillard, and V. Dousset. “Macrophage Imaging in Central Nervous System and in Carotid Atherosclerotic Plaque Using Ultrasmall Superaparamagnetic Iron Oxide in Magnetic Resonance Imaging,” *Investigative Radiology*, **39** (2004) 619-625.

21. McCarthy, J. R. and R. Weissleder. “Multifunctional magnetic nanoparticles for targeted imaging and therapy,” *Advanced Drug Delivery Reviews*, **60** (2008) 1241-1251.

22. Saini V., V. P. Zharov, C. S. Brazel, D. E. Nikles, D. T. Johnson, and M. Everts. “Combination of viral biology and nanotechnology: new applications in nanomedicine,” *Nanomedicine: Nanotechnology, Biology and Medicine*, **2** (2006) 200-206.

23. McCarthy, J. R., K. A. Kelly, E. Y. Sun, and R. Weissleder. “Targeted delivery of multifunctional magnetic nanoparticles,” *Nanomedicine*, **2** (2007) 153-167.

24. Gupta, A. K., R. R. Naregalkar, V. D. Vaidya, and M. Gupta. “Recent advances on surface engineering of magnetic iron oxide nanoparticles and their biomedical applications,” *Nanomedicine,* **2** (2007) 23-39.

25. Ito, A., M. Shinkai, H. Honda, T. Kobayashi. “Medical applications of functional magnetic nanoparticles,” *Journal of Bioscience and Bioengineering*, **100** (2005) 1-11.

26. Weber, C. and D. Falkenhagen, “Specific blood purification by means of antibody conjugated magnetic microspheres,” in: U. Hafeli, et al., (Eds.), *Scientific and Clinical Applications of Magnetic Carriers, Plenum Press*, New York, 1997.

27. J. M. Nam, C. S. Thaxton, and C. A. Mirkin, “Nanoparticle-based bio-bar codes for the ultrasensitive detection of proteins,” *Science* **301** (2003) 1884–1886.

28. Schroeder, U., P. Sommerfeld, S. Ulrich, and B. A. Sabel. “Nanoparticle technology for delivery of drugs across the blood–brain barrier,” *Journal of Pharmaceutical Sciences*, **87** (1998) 1305–1307.

29. Vega-Villa, K. R., J. K. Takemoto, J. A. Yáñez, C. M. Remsberg, M. L. Forrest, and N. M. Davies. “Clinical toxicities of nanocarrier systems,” *Advanced Drug Delivery Reviews*, **60** (2008) 929-938.

30. Pankhurst, Q.A., J. Connolly, S.K. Jones, and J. Dobson. “Applications of Magnetic Nanoparticles in Biomedicine,” *Journal of Physics D: Applied Physics*, **36** (2003) R167-R181.

31. Hasegawa, M., T. Hanarch, H. Shoji, T. Kawaguchi, and S. Maruno. “Biological behavior of dextran-iron oxide magnetic fluid injected intravenously in rats,” *Japanese Journal of Applied Physics*, **37** (1998) 1029-1032.

32. Kim, D.-H., D. E. Nikles, D. T. Johnson, and C.S. Brazel. “Heat generation of aqueously dispersed $CoFe_2O_4$ nanoparticles as heating agents for magnetically-activated drug delivery and hyperthermia,” *Journal of Magnetism and Magnetic Materials*, **320** (2008) 2390-2396.

33. Kim, D.-H., S.-H. Lee, K.-H. Nam, K.-M. Kim, I.-B. Shim, and Y.-K. Lee. “Cytotoxicity of ferrite particles by MTT and agar diffusion methods for hyperthermic applications,” *Journal of Magnetism and Magnetic Materials*, **293** (2005) 287-292.

34. Kim, D.-H., Y. T. Thai, D. E. Nikles, and C. S. Brazel. “Heating of Aqueous Dispersions Containing $MnFe_2O_4$ Nanoparticles by Radio-Frequency Magnetic Field Induction,” *IEEE Transactions on Magnetics*, **45** (2009) 64-70.

35. Brezovich, I.A. “Low frequency hyperthermia: capacitive and ferromagnetic thermoseed methods,” *Medical Physics Monograph*, **16** (1988) 82-111.

36. Simon, M. and J. S. Mattson. The pioneers of NMR and magnetic resonance in medicine: The story of MRI. Gan, Israel: Bar-Ilan University Press, 1996.

37. Kim, D.-H. and C. S. Brazel. "T1 and T2 Relaxivities of Succimer-coated MFe23+O4 (M = Mn2+, Fe2+ and Co2+) Inverse Spinel Ferrites for Potential use as Phase Contrast Agents in Medical MRI," *Journal of Magnetism and Magnetic Materials, Article In Press* (2009)

38. Bertorelle, F., C. Wilhelm, J. Roger, F. Gazeau, C. Ménager, and V. Cabuil. "Fluorescence-Modified Superparamagnetic Nanoparticles: Intracellular Uptake and Use in Cellular Imaging," *Langmuir*, **22** (2006) 5385-5391.

39. Brazel, C. S., I. Ankareddi, M. L. Hampel, H. Bagaria, D. T. Johnson and D. E. Nikles. "Development of magnetothermal-responsive delivery systems using FePt nanoparticles imbedded in poly(*N*-isopropylacrylamide)-based hydrogels," *Control. Rel. Soc. Trans.*, **33** 2006 762.

40. Curtis, J., M. Greenberg, J. Kester, S. Phillips, and G. Krieger. "Nanotechnology and nanotoxicology: a primer for clinicians," *Toxicological Reviews*, **25** (2006) 245–260.

41. Zhang, K., H. Fang, R. Rossin, Z. Chen, J. A. Taylor, M. J. Welch, and K. L. Wooley. "Cell Uptake and the Dependency on Surface Moieties of Differently-shaped Nanoparticles," *Polymeric Materials: Science and Engineering*, **99** (2008) 727.

42. Cotter, T. G. and M. Al-Rubeai. "Cell death (apoptosis) in cell culture systems," *Trends in Biotechnology*, **13** (1995) 150-155.

43. Kim, D.-H., K.-N. Kim, K.-M. Kim, I.-B. Shim, and Y.-K. Lee. "*In vitro* and *in vivo* toxicity of $CoFe_2O_4$ for application to magnetic hyperthermia," *NSTI-Nanotech*, **2** (2007) 748-751.

44. Becker, C., M. Hodenius, G. Blendinger, A. Sechi, T. Hieronymus, D. Müller-Schulte, T. Schmitz-Rode, and M. Zenke. "Uptake of magnetic nanoparticles into cells for cell tracking," *Journal of Magnetism and Magnetic Materials*, **311** (2007) 234-237.

45. Hagens, W. I., A. G. Oomen, W. H. de Jong, F. R. Cassee, A. J.A.M. Sips. "What do we (need to) know about the kinetic properties of nanoparticles in the body?," *Regulatory Toxicology and Pharmacology*, **49** (2007) 217-299.

46. Hillyer, J. F. and R. M. Albrecht. "Gastrointestinal Persorption and Tissue Distribution of Differently Sized Colloidal Gold Nanoparticles," *Journal of Pharmaceutical Sciences*, **90** (2001) 1927-1936.

47. Kuckelhaus, S., S. C. Reis, M. F. Carnerio, A. C. Tedesco, D. M. Oliveira, E. C. D. Lima, P. C. Morais, R. B. Azevedo, and Z. G. M. Lacava. "In vivo investigation of cobalt ferrite-based magnetic fluid and magnetoliposomes using morphological tests," *Journal of Magnetism and Magnetic Materials*, **272-276** (2004) 2402-2403.

48. Huang, X.-L., B. Zhang, L. Ren, S.-F. Ye, L.-P. Sun, Q.-Q. Zhang, M.-C. Tan, and G.-M. Chow. "In vivo toxic studies and biodistribution of near infrared sensitive Au-Au_2S nanoparticles as potential drug delivery carriers," *Journal of Materials Science: Materials in Medicine*, **19** (2008) 2581-2588.

49. Fabian, E., R. Landsiedel, L. Ma-Hock, K. Wiench, W. Wohlleben, B. van Ravenzwaay. "Tissue distribution and toxicity of intravenously administered titanium dioxide nanoparticles in rats," *Archives of Toxicology.*, **82** (2008) 151-157.

50. Wilhelm, C., F. Gazeau, J. Roger, J. N. Pons, and J. C. Bacri. "Interaction of Anionic Superparamagnetic Nanoparticles with Cells: Kinetic Analyses of Membrane Adsorption and Subsequent Internalization," *Langmuir*, **18** (2002) 8148-8155.

51. Raynal, I., P. Prigent, S. Peyramaure, A. Najid, C. Rebuzzi, and C. Corot. "Macrophage Endocytosis of Superparamagnetic Iron Oxide Nanoparticles: Mechanisms and Comparison of Ferumoxides and Ferumoxtran-10," *Investigative Radiology*, **39** (2004) 56-63.

52. Garnett, M. C. and P. Kallinteri. "Nanomedicines and nanotoxicology: some physiological principles," *Occupational Medicine*, **56** (2006) 307-311.

53. Wilhelm, C., C. Billotey, J. Roger, J. N. Pons, J.-C. Bacri, and F. Gazeau. "Intracellular uptake of anionic superparamagnetic nanoparticles as a function of their surface coating," *Biomaterials*, **24** (2003) 1001-1011.

54. Rogers, W. J., and P. Basu. "Factors regulating macrophage endocytosis of nanoparticles: implications for targeted magnetic resonance plaque imaging," *Atherosclerosis*, **178** (2005) 67-73.

55. Jordan, A., R. Scholz, P. Wust, H. Schirra, T. Schiestel, H. Schmidt, and R Felix. "Endocytosis of dextran and silan-coated magnetite nanoparticles and the effect of intracellular hyperthermia on human mammary carcinoma cells in vitro," *Journal of Magnetism and Magnetic Materials*, **194** (1999) 185-196.

56. Nahta, R. and F. J. Esteva. "Herceptin: mechanisms of action and resistance," *Cancer Letters*, **232** (2006) 123-138.

57. Schmaljohann, D. "Thermo- and pH-responsive polymers in drug delivery," *Advanced Drug Delivery Reviews*, **58** (2006) 1655-1670.

58. Sun, S. H. Zeng, D.B. Robinson, S. Raous, P.M. Rice, S.X. Wang, and G. Li. "Monodisperse MFe_2O_4 (M= Fe, Co, Mn) Nanoparticles," *Journal of the American Chemical Society*, **126** (2004), 273-279.

59. Personal communication with Maaike Everts, February 2009.

60. Thorek, D. L. J. and A. Tsourkas. “Size, charge and concentration dependent uptake of iron oxide particles by non-phagocytic cells,” *Biomaterials,* **29** (2008) 3583-3590.

61. Pisanic II, T. R., J. D. Blackwell, V. I. Shubayev, R. R. Fiñones, and S. Jin. “Nanotoxicity of iron oxide nanoparticles internalization in growing neurons,” *Biomaterials,* **28** (2007) 2572-2581.

62. Enlander, D., P. M. Weber, and L. V. dos Remedios. “Renal Cortical Imaging in 35 Patients: Superior Quality with ^{99m}Tc-DMSA,” *The Journal of Nuclear Medicine*, **15** (1974) 743-749.

63. Wang, S. C., K. S. Ting, and C. C. Wu. “Chelating therapy with NA-DMS in occupational lead and mercury intoxications,” *Journal of Chinese Medicine*, **84** (1965) 437-439.

64. Mallinckrodt Baker, Inc. “Material Safety Data Sheet: Rhodamine B, # R5400.” <http://www.jtbaker.com/msds/englishhtml/r5400.htm>.

65. Rasband, W.S., ImageJ, U. S. National Institutes of Health, Bethesda, Maryland, USA, 1997-2008, <http://rsb.info.nih.gov/ij/>.

66. Wilhelm, C. and F. Gazeau. “Universal cell labeling with anionic magnetic nanoparticles,” *Biomaterials,* **29** (2008) 3161-3174.

67. Hussain, S. M., A. K. Javorina, A. M. Schrand, H. M. Duhart, S. F. Ali, and J. J. Schlager. “The Interaction of Manganese Nanoparticles with PC-12 Cells Induces Dopamine Depletion,” *Toxicological Sciences*, **92** (2006) 456-463.

68. Clokey, G. V. and L. A. Jacobson. “The Autoflourescent “Liposfuscin Granules” in the Intestinal Cells of *Caenorhabditis Elegans* are Secondary Lysosomes,” *Mechanisms of Ageing and Development*, **35** (1986) 79-94.

69. Long, X., C. Spycher, Z. S. Han, A. M. Rose, F. Müller, and J. Avruch. “TOR Deficiency in *C. elegans* Causes Developmental Arrest and Intestinal Atrophy by Inhibition of mRNA Translation,” *Current Biology*, **12** (2002) 1448-1461.

70. Bagaria, H. Unpublished data from PhD research at The University of Alabama under D. T. Johnson.

APPENDIX 1

Procedure for Staining Cells with Phalloidin (Alexa® Fluor 488)

Before removing cultures from the incubator, allow the stains and fixing reagents to warm to room temperature. Also, during soaking or fixing steps, be sure to keep cultures covered to minimize chance of samples drying out.

Reagents needed for phalloidin (Alexa Fluor 488) staining procedure: 1X Phosphate Buffer Solution (PBS), 3.7 % formaldehyde in PBS, 0.1% Triton-X in PBS, and methanol-phalloidin stock solution.

1. After removing cultures to be stained from incubator, remove media (or media and MNP) from chambers by vacuuming, being careful not to touch the bottom of the slide where the cells are adhered.

2. Wash the culture twice using 1X PBS. Pipette enough PBS into the chamber to cover the bottom of the slide, again being careful not to touch the slide where cells are adhered. Vacuum off the PBS after each wash.

3. Fix the cells by using the 3.7% formaldehyde in PBS for 10 min. Use enough of the solution to cover the bottom of the slide where cells are adhered. Vacuum off solution after 10 min, then wash twice with PBS.

4. Submerge the chamber in enough 1.0% Triton-X in PBS to cover the adherent cells on the bottom of the slide. Let soak for 5 min, then vacuum off solution. Wash twice with PBS.

5. Dilute methanol-phalloidin stock solution in PBS at a 1:40 volume ratio. Use at least 200 μL per well to be stained. Using more stain (or a higher ratio of stain to PBS) will give a more intense signal in the fluorescent images.

6. Submerge the chamber in at least 200 μL of the staining solution for 20 min. The bottom of the slide, where cells are adhered, should be completely covered by the solution. Vacuum off staining solution and wash sample twice with PBS.

APPENDIX 2

Data and Sample Calculations for Studies of Rhodamine-MNP Bond Stability

For analysis, dilutions of Sample 4 were analyzed.

Concentration: 0.05 mg/mL

Volume: 5 mL

Total mass of rhodamine-tagged MNPs in sample: 0.25 mg

Sample Calculation for mass of free rhodamine per mass MNP:

Average concentration of free rhodamine for room temperature sample: 0.0005 mg/mL

Average mass of free rhodamine in 5 mL sample: 0.0025 mg

Mass free rhodamine per mass MNPs:

$$= \frac{\text{Mass Free Rhodamine}}{\text{Mass MNPs}} = \frac{0.0025\,\text{mg}}{0.25\,\text{mg}} = 0.010\,\text{mg free rhodamine per mg MNPs}$$

Room Temperature Sample: 0.010 ± 0.0005 mg free rhodamine per mg MNPs

37 ^{o}C Sample: 0.010 ± 0.0001 mg free rhodamine per mg MNPs

Table A2.1 Data Used to Determine Ratio of Free Rhodamine to MNPs in Solution

Room Temperature

	Concentration Free Rhodamine (mg/mL)	Mass Free Rhodamine (mg)	Mass Free Rhodamine per mass MNP
Trial 1	0.0006	0.0028	0.011
Trial 2	0.0006	0.0028	0.011
Trial 3	0.0005	0.0026	0.010
Trial 4	0.0005	0.0025	0.010
Trial 5	0.0005	0.0025	0.010
Average	0.0005	0.0026	0.011

37 ^{o}C

	Concentration Free Rhodamine (mg/mL)	Mass Free Rhodamine (mg)	Mass Free Rhodamine per mass MNP
Trial 1	0.0005	0.0025	0.010
Trial 2	0.0005	0.0024	0.010
Trial 3	0.0005	0.0024	0.010
Trial 4	0.0005	0.0024	0.009
Trial 5	0.0005	0.0023	0.009
Average	0.0005	0.0024	0.010

APPENDIX 3

$CoFe_2O_4$ MNP Localization in HeLa Cell Data and Partition Coefficient Sample Calculations

30 min Incubation Time:

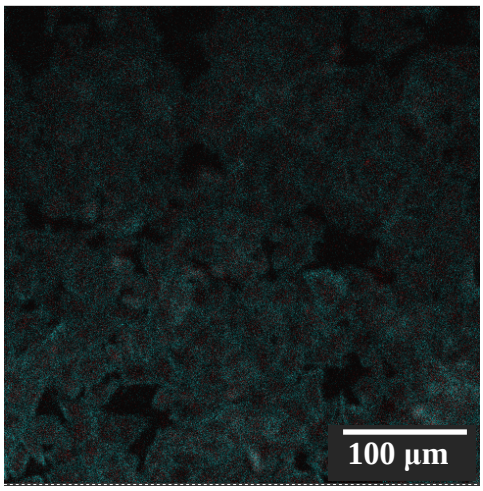

(a)

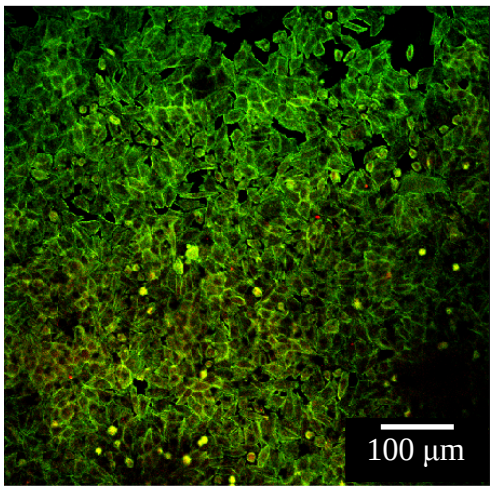

(b)

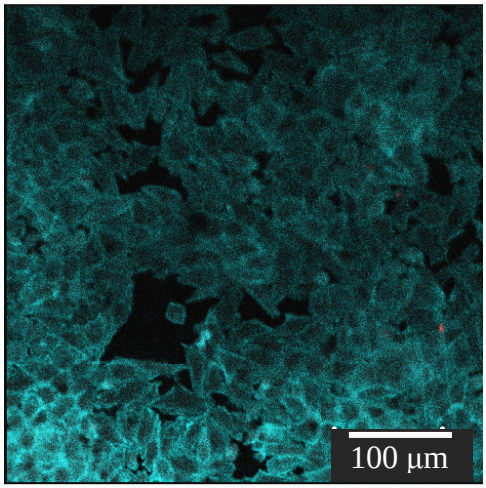

(c)

Figure A3.1 Confocal Microscope Images of HeLa Cells Exposed to 10% Rhodamine-Tagged $CoFe_2O_4$ MNPs for 30 min. Images Represent Overlays of Green and Red Channels from Confocal Microscope at 20X Magnification.

Table A3.1 Data from ImageJ for HeLa Cells Incubated with $CoFe_2O_4$ MNPs for 30 min

	Image A	**Image B**	**Image C**
Fluorescence In Cells	3.444	435.200	4003.419
Fluorescence Outside Cells	39.600	5632.000	42680.588
Total Area of Cells	125300.689	219496.960	28717.143
Total Area Outside Cells	51310.992	104106.454	8292.823
K	0.036	0.037	0.027

Average K: 0.033 ± 0.005

2 h Incubation Time:

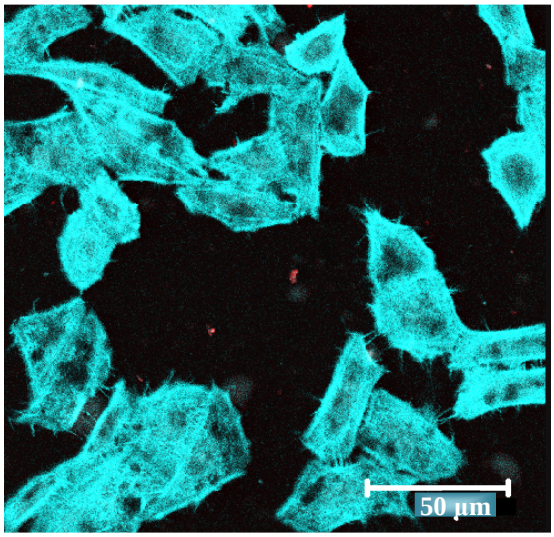

(a)

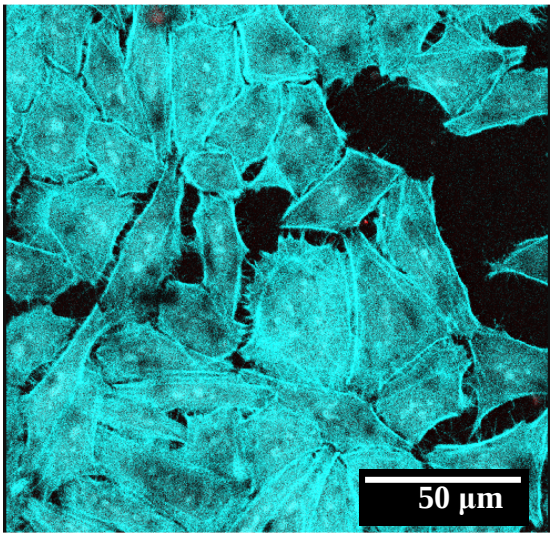

(b)

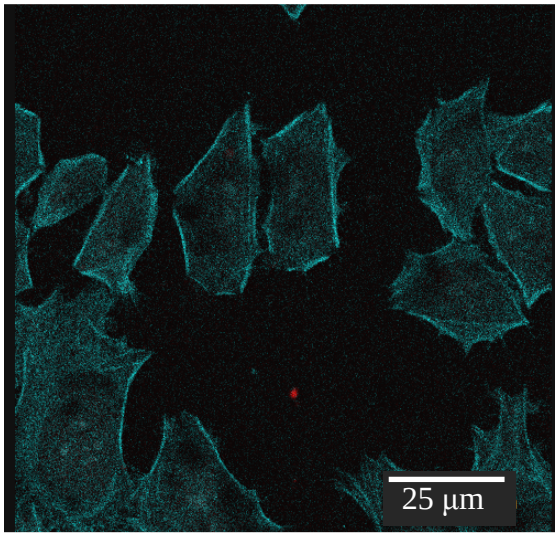

(c)

Figure A3.2 Confocal Microscope Images of HeLa Cells Exposed to 10% Rhodamine-Tagged $CoFe_2O_4$ MNPs for 2 h. Images Represent Overlays of Green and Red Channels from Confocal Microscope at (a) and (b) 63X Magnification and (c) 100X Magnification.

Table A3.2 Data from ImageJ for HeLa Cells Incubated with $CoFe_2O_4$ MNPs for 2 h

	Image A	**Image B**	**Image C**
Fluorescence In Cells	25.109	3.874	6.119
Fluorescence Outside Cells	21.809	2.296	7.843
Total Area of Cells	14048.067	25141.041	6213.455
Total Area Outside Cells	15364.577	8884.377	6902.571
K	1.259	0.596	0.867

Average K: 0.907 ± 0.333

6 h Incubation Time:

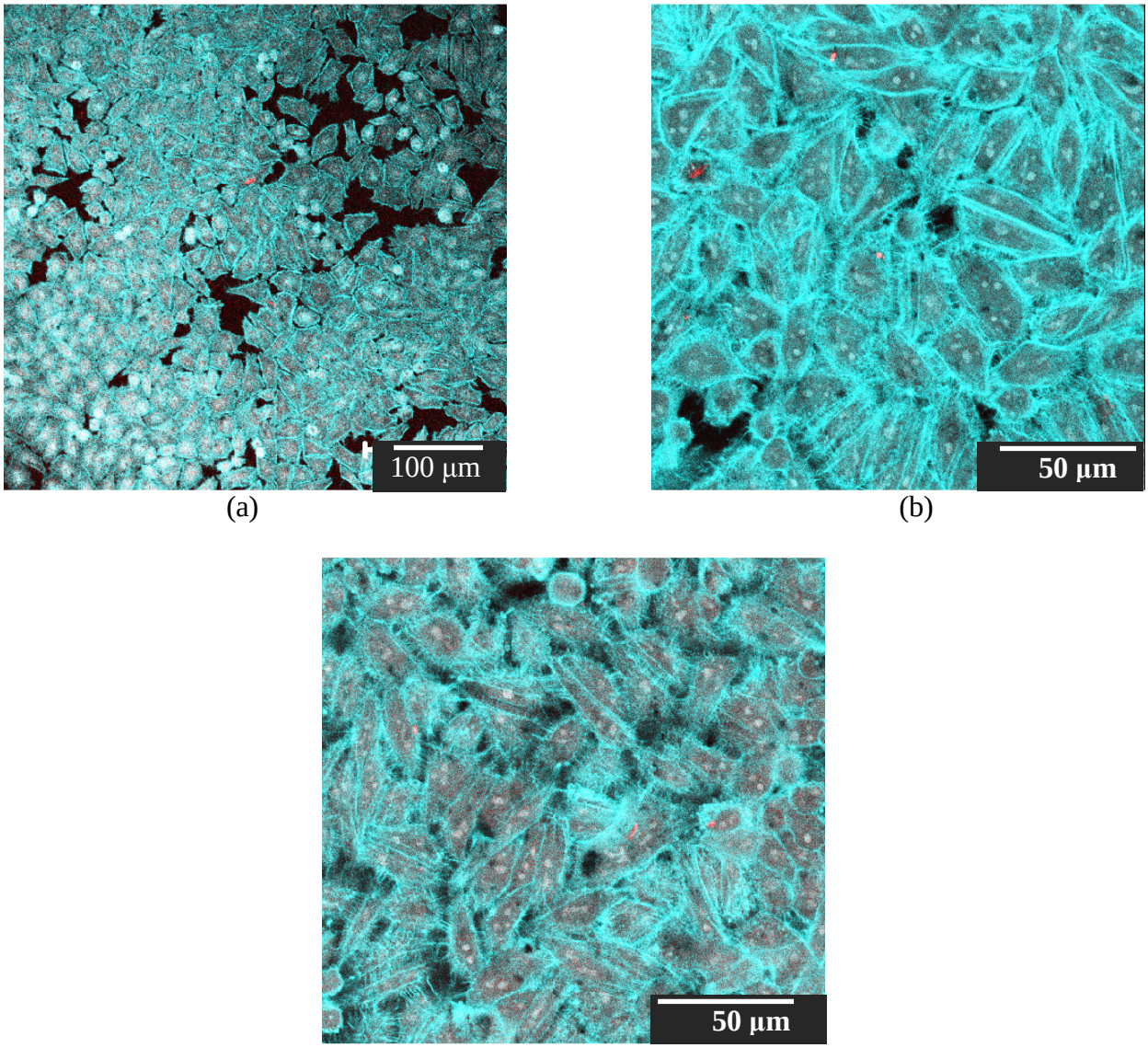

(a) (b)

Figure A3.3 Confocal Microscope Images of HeLa Cells Exposed to 10% Rhodamine-Tagged $CoFe_2O_4$ MNPs for 6 h. Images Represent Overlays of Green and Red Channels from Confocal Microscope at (a) 20X Magnification and (b) and (c) 63X Magnification.

Table A3.3 Data from ImageJ for HeLa Cells Incubated with $CoFe_2O_4$ MNPs for 6 h

	Image A	**Image B**	**Image C**
Fluorescence In Cells	27227.244	175470.525	1519.098
Fluorescence Outside Cells	2025.798	7301.244	95.673
Total Area of Cells	255179.827	27515.669	26687.635
Total Area Outside Cells	72103.872	4577.066	6086.079
K	3.798	3.998	3.621

Average K: 3.805 ± 0.189

24 h Incubation Time:

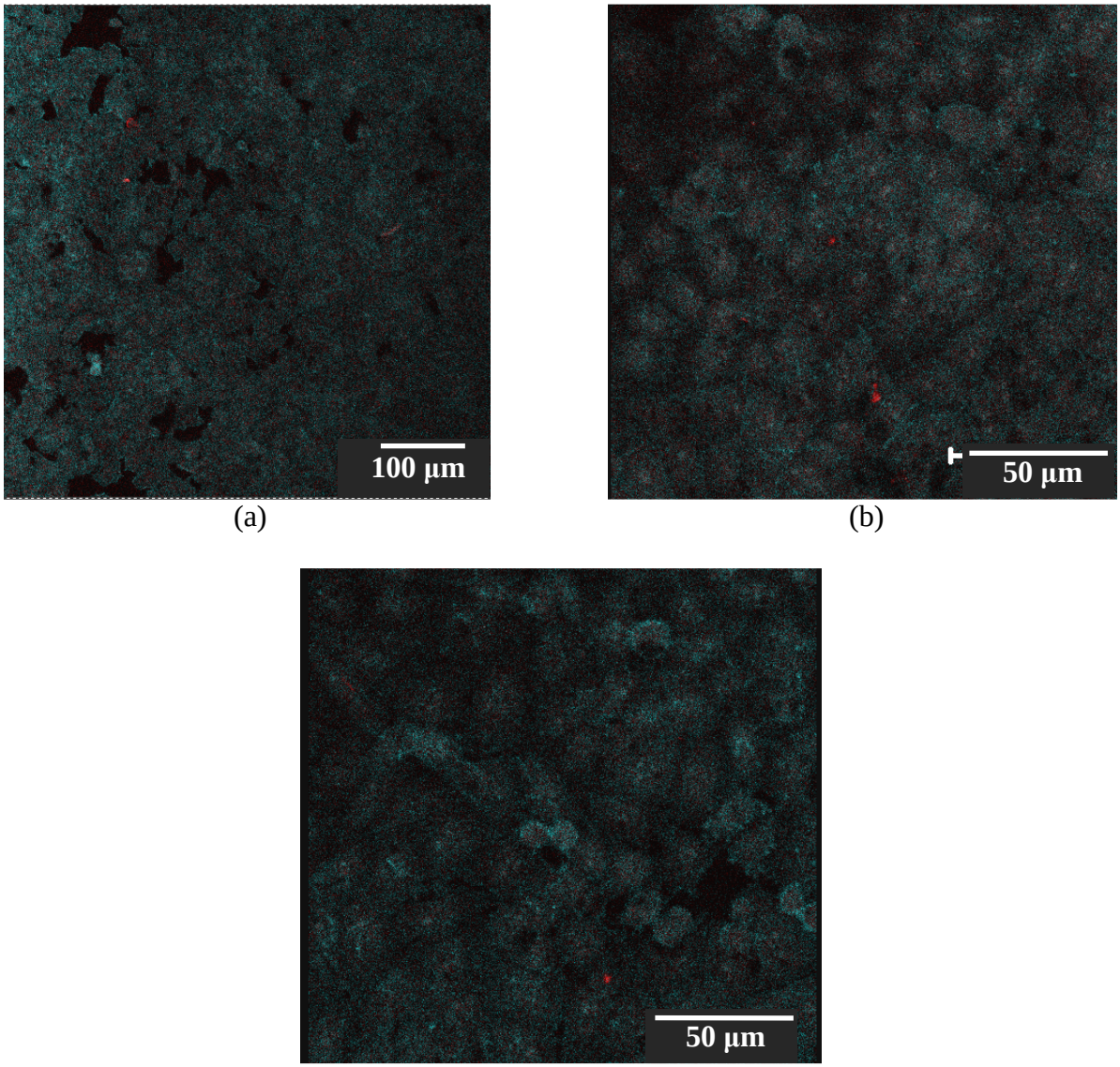

(a) (b)

Figure A3.4 Confocal Microscope Images of HeLa Cells Exposed to 10% Rhodamine-Tagged $CoFe_2O_4$ MNPs for 24 h. Images Represent Overlays of Green and Red Channels from Confocal Microscope at (a) 20X Magnification and (b) and (c) 63X Magnification.

Table A3.4 Data from ImageJ for HeLa Cells Incubated with $CoFe_2O_4$ MNPs for 24 h

	Image A	**Image B**	**Image C**
Fluorescence In Cells	12666.294	7906.049	7723.094
Fluorescence Outside Cells	2941.058	1812.012	1429.150
Total Area of Cells	209991.888	25904.068	26132.203
Total Area Outside Cells	82349.703	7009.212	8882.071
K	1.689	1.181	1.837

Average K: 1.569 ± 0.344

Sample Calculations for Partition Coefficient, K

$$K = \frac{A_{RC} / A_C}{A_{RO} / A_O}$$

Use data from 2 h Incubation Time, Figure A3.2a

Area of Red Fluorescence Inside Cells, A_{RC} = 25.109

Area of Cells, A_C = 14048.067

Area of Fluorescence Outside Cells, A_{RO} = 21.809

Area Outside of Cells, A_O = 15364.577

$$K = \frac{25.109 / 14048.067}{21.809 / 15364.577} = 1.259$$

APPENDIX 4

Discussion of Results from Localization and Uptake of Rhodamine-Tagged $CoFe_2O_4$ MNPs in *C. elegans* Worms

The wild type and mutant *C. elegans* worms were fixed to a glass slide with levamisole (Sigma-Aldrich Chemical Co., St. Louis, MO)) on an agar pad. Slides were analyzed using a Nikon E800 fluorescent microscope (Nikon Corporation, Melville NY) and the confocal microscope also used in the HeLa studies.

Before an in depth analysis of the results, the technical difficulties associated with these experiments will be discussed. After obtaining the images of the wild type and mutant worms, two significant problems became apparent: bleed over and autofluorescence. Bleed over in confocal microscopy occurs when a fluorophore is over excited, allowing fluorescence to "leak" into a channel in which the fluorophore does not actually fluoresce. Bleed over can be caused by prolonged exposure to the lasers used by the confocal microscope for exciting the stains. Bleed over can also be induced by exposing the mutant *C. elegans* specimens to the light in the green channel first. In these experiments, the 488 nm light used to visualize the green fluorescent protein expressed within the neurons of the mutant *C. elegans* may have accidentally over excited the neurons and caused fluorescence to appear in the neurons when viewed in the red channel for visualizing rhodamine-tagged MNPs. The term autofluorescence refers to any natural fluorescence of a specimen, rather than fluorescence induced by staining or tagging the samples with fluorescent moieties. The intestine and gut granules of *C. elegans* can autofluoresce when stimulated by a variety of wavelengths [68].

In the wild-type *C. elegans* worms that were fed rhodamine-tagged $CoFe_2O_4$, the MNPs appeared to have localized in head, midsection, and tails of the worms (Figure A4.1a and b) although autofluorescence and bleed over prevent these images from being conclusive. The majority of the red fluorescence was localized in the gastrointestinal (GI) tract of the worms. The image of a whole worm clearly shows the mouth, pharynx, and GI tract with red fluorescence (Figure A4.1a). In Figure A.4b, there is a magnification of the midsection of the worm, showing the GI tract and the ventral neural cords. In the worm intestine, an uneven distribution of red fluorescence is seen. The pattern suggests that the fluorescent MNPs may have been absorbed through the lumen tissue of the worm and into the intestinal tissues. The areas of highest intensity could be gut granules, which are organelles related to lysosomes in the alimentary canal of the worm. Several control wild type *C. elegans* worms that were not fed the rhodamine-tagged MNPs did not show bright and clear images of the autofluorescing gut granules when viewed under the same conditions as the experimental worms (Figure A4.2a). However, autofluorescence varied from worm to worm even when viewed at the same settings on the confocal microscope (Figure A4.2b). Images obtained of the worms fed rhodamine-tagged MNPs typically showed much higher intensities of red fluorescence in the intestinal lumen and gut granules than the control worms. This appears to support the suggestion that rhodamine-tagged $CoFe_2O_4$ may localize in the intestinal tissues and gut granules of the worms. Work conducted by Clokey and Jacobson shows that the gut granules of *C. elegans* worms endocytose rhodamine-tagged bovine serum albumin microspheres with diameters around 0.25 μm [68]. This suggests that despite autofluorescence of the intestines, the uptake of rhodamine-tagged $CoFe_2O_4$ MNPs through the lumen and into the surrounding intestinal tissue is possible. The rhodamine-tagged MNPs could localize in the gut granules because the granules function as

a secondary lysosome for the worm for fat storage and some catabolic processes [68]. Another group reports negligible autofluorescence of the worm intestine when viewed in the rhodamine channel of a fluorescence microscope, and that the intestine and gut granules were only visible in the red channel if the worm was fed Neutral Red dye [69]. Further work, including a better study of a group of control worms, is needed to conclusively determine the localization of the MNPs in the worms. The discussion of results below incorporates the assumption that the autofluorescence of the worm is much lower in intensity than the fluorescence from the nanoparticles.

The localization studies of rhodamine-tagged MNPs in wild type *C. elegans* worms were also used to screen for toxicity of the samples, as well as a starting point for further work with mutant *C. elegans*. After two days exposure to the MNPs, the worms were still capable of reproducing indicating little toxicity. Results from the rhodamine-tagged MNP localization in wild type *C. elegans* worms build on results from previous studies involving iron platinum, FePt, MNPs [70]. In these studies, wild type *C. elegans* were exposed to FePt nanoparticles as a part of their feed with the MNPs being localized in the intestinal lumen of the worms (A4.3b and c). The FePt MNPs have aggregated and appear to only be localized in the lumen, which supported the thought that the MNPs could not be passed through the tissue and into surrounding spaces of the worm (A4.3c). However, the rhodamine-tagged $CoFe_2O_4$ studies allowed for a more complete visualization of the worms exposed to MNPs. The results from this study indicate that it might be possible for rhodamine-tagged $CoFe_2O_4$ MNPs to pass through the intestinal lumen, into the intestinal tissues and localize to cells and organelles present there. Because of the complication from autofluorescence, more work is needed to conclusively determine the localization of rhodamine-tagged $CoFe_2O_4$ MNPs in these organisms.

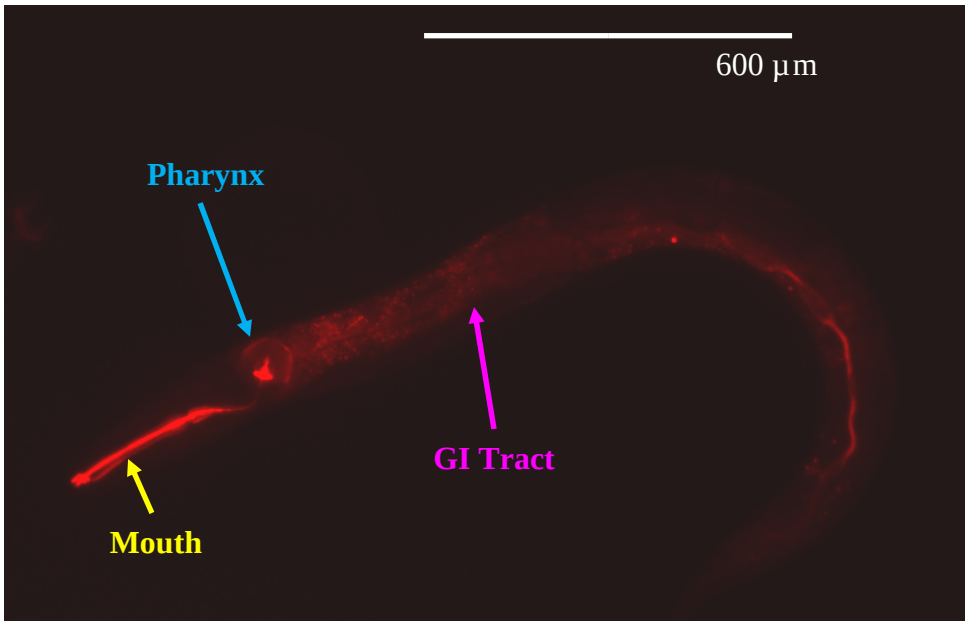

(a)

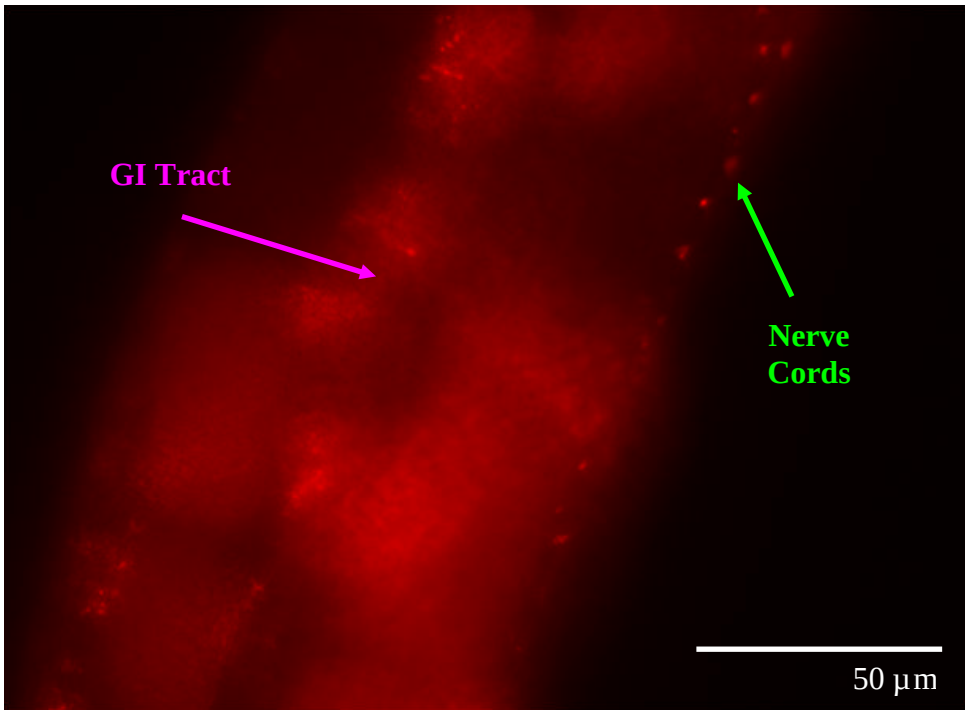

(b)

Figure A4.1 Fluorescence Microscope Images of a Wild Type *C. elegans* Worm After 2 Days of Exposure to Rhodamine-Tagged $CoFe_2O_4$ MNPs: (a) Whole Worm at 10X Magnification, (b) 100X Magnification of Ventral Neural Cords. Representative Images Shown.

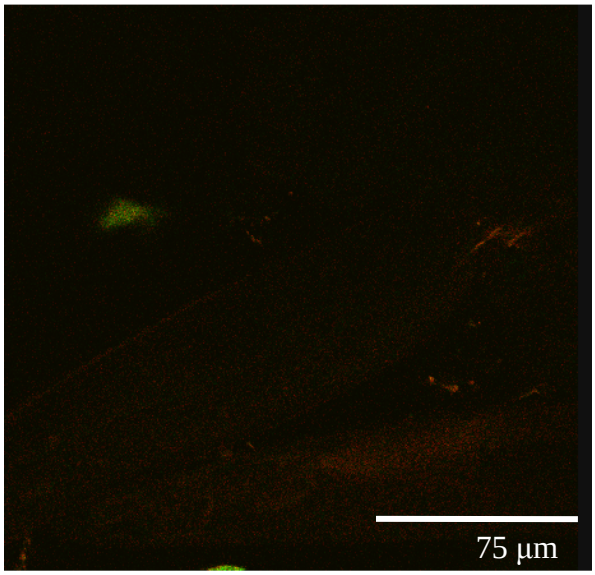

(a)

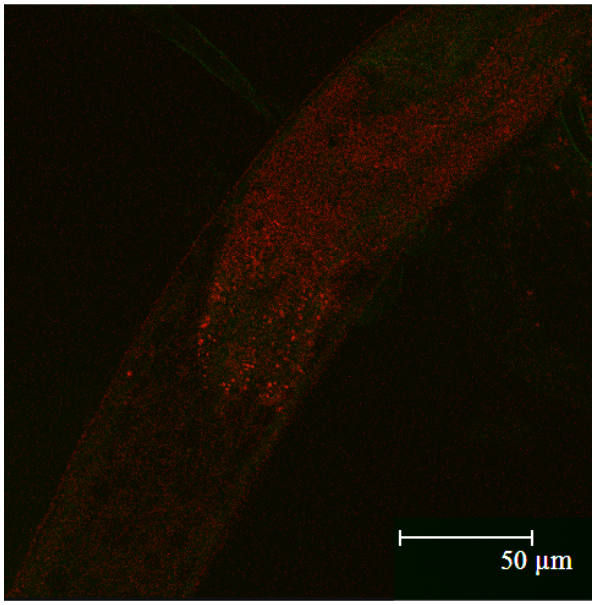

(b)

Figure A4.2 Confocal Microscope Images of Control Wild Type *C. elegans* Worms. Images Represent Overlay of Green and Red Channels at 63X Magnification. Scale Bars are Approximate. Representative Images Shown.

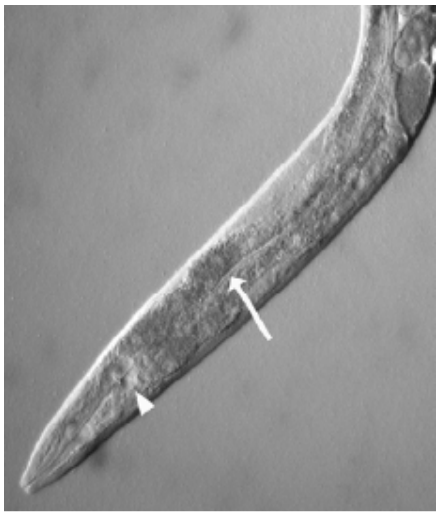

(a)

(b)

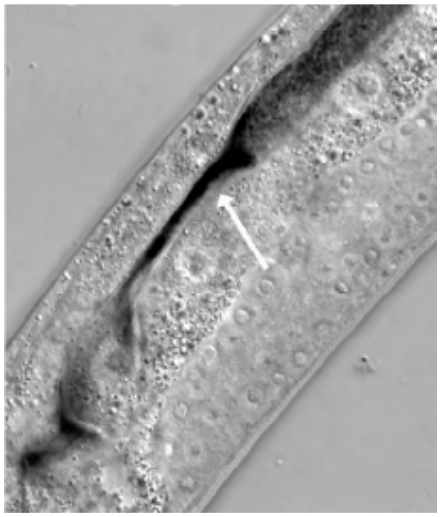

(c)

Figure A4.3 Microscope Images of Wild Type *C. elegans* Worm After Exposure to FePt MNPs: (a) Control Worm, no MNPs, (b) After 72 h Exposure to FePt MNPs, and (c) Magnification of GI Tract of Worm with FePt MNPs. Images Reproduced from Unpublished Work by H. Bagaria [70].

To investigate the possible localization of rhodamine-tagged $CoFe_2O_4$ MNPs in the nervous networks of the *C. elegans* worms, a strand of mutant worms, which have a green fluorescing protein to label their neurons, was also fed rhodamine-tagged $CoFe_2O_4$ MNPs. The study with the mutant worms was prompted by evidence that rhodamine-tagged MNPs may have localized in the neurons of wild type *C. elegans* (Figure A4.1b). After the studies with the mutant worms were begun, the fluorescence seen in the neurons in A4.1b was attributed to bleed over. Confocal microscopy images of mutant worms with rhodamine-tagged MNPs were collected. However, because of the bleed over problem discussed in earlier in this appendix, no conclusions could be drawn from these studies. While mutant worms show colocalization of red and green fluorescence after 24 h and 12 d exposure times, it cannot be definitively attributed to the localization of nanoparticles in the neurons (A4.4 and A4.5).

The GI tract of the worms showed similar red fluorescence patterns as found in the wild type studies, indicating that the MNPs may have been absorbed through the lumen and localized by the gut granules. After 24 h, most of the red fluorescence was most prominent in the intestinal tissue of the worm (Figure A4.4a). *C. elegans* worms that had been exposed to rhodamine-tagged MNPs for 12 days showed similar results with red fluorescence indicating: possible accumulation of MNPs in the gut granules and some colocalization of red and green fluorescence in the neurons (A4.5a and b). Magnifications of the heads of the worms show areas of both green and red fluorescence, visualized as yellow (Figure A4.4b and A4.5b). From the images obtained, there is no way to determine if the fluorescence corresponds to nanoparticles or over-excited neurons. Because bleed over cannot be ruled out as the cause of the colocalization of green and red fluorescence in these worms, no quantitative analysis of these images is reported. Appendix 5 includes a discussion about how to utilize ImageJ to determine the relative

colocalization of rhodamine-tagged $CoFe_2O_4$ nanoparticles in the neurons of worms, if the effects of bleed over and autofluorescence can be decoupled from the fluorescence due to the MNPs.

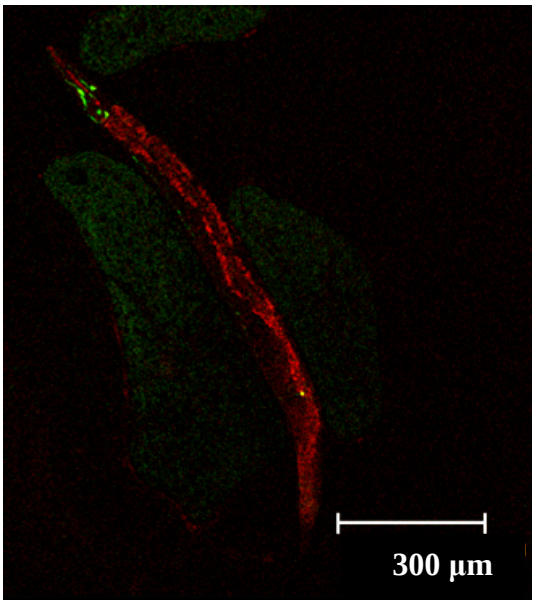

(a)

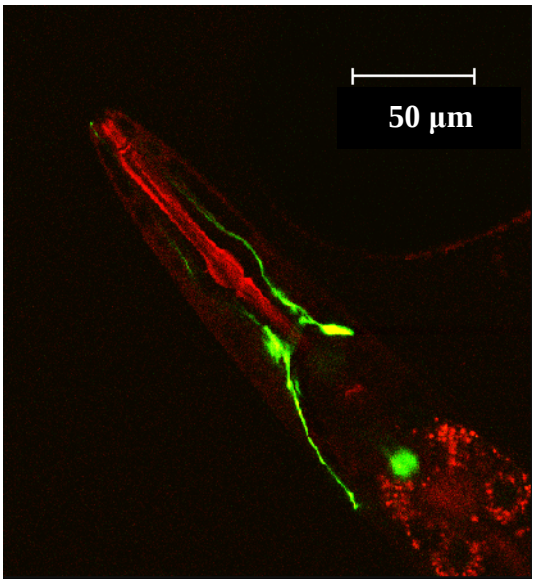

(b)

Figure A4.4 Confocal Microscope Images of Mutant *C. elegans* Worms After 24-Hour Exposure to Rhodamine-Tagged $CoFe_2O_4$ MNPs: (a) Whole Worm at 10X Magnification, (b) Head of Worm at 63X Magnification. The amorphous shapes present in 6.21a are Bubbles in the Embedding Media. Representative Images Shown.

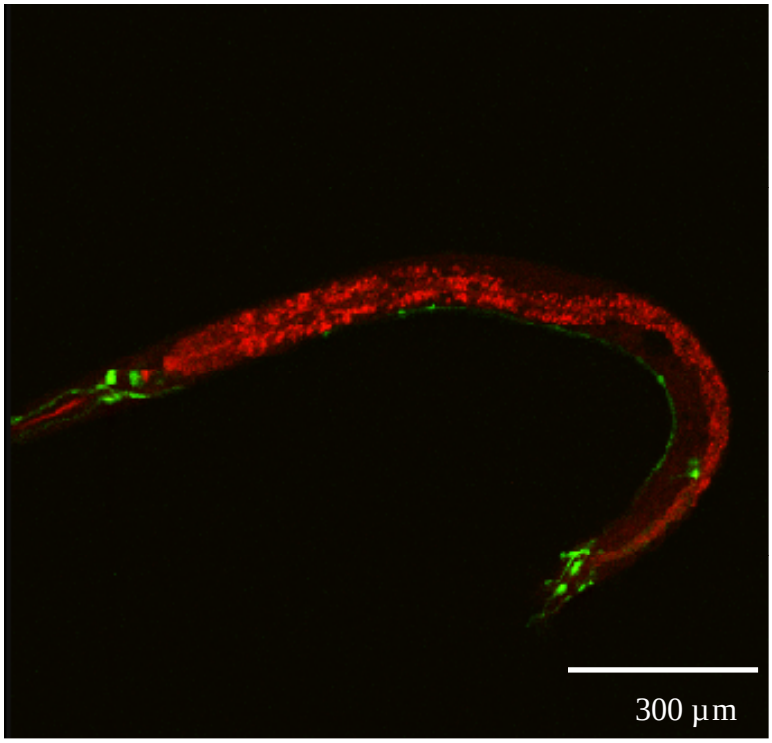

(a)

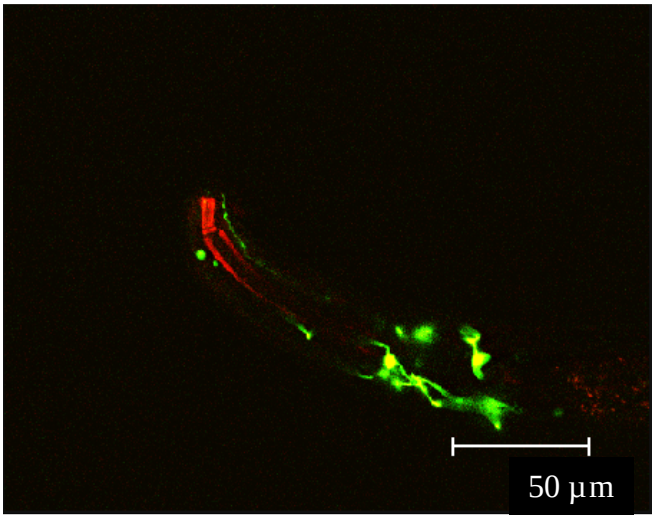

(b)

Figure A4.5 Confocal Microscope Images of Mutant *C. elegans* Worms After 12-Day Exposure to Rhodamine-Tagged $CoFe_2O_4$ MNPs: (a) Whole Worm at 20X, (b) Head of Worm at 63X. Representative Images Shown.

APPENDIX 5

Recommended Protocol for Studying MNP Localization in Neurons of *C. elegans* Worms

To obtain images that can provide definitive data about whether or not rhodamine-tagged $CoFe_2O_4$ MNPs can localize to the neurons of *C. elegans* worms, a better defined experimental procedure is required. The procedure described below includes careful control of specimens, so that the only difference between the control and experimental groups is the presence of fluorescent MNPs in the food for the experimental group. While the protocol that follows is specifically designed for mutant worms used in these studies, it can be adapted for other types of worms as well.

The proposed experiment to study colocalization of MNPs in the neurons of the worms utilizes two groups of mutant worms: a control group and a MNP group. Both sets should exhibit the same mutation which causes the green fluorescence of neurons. The *C. elegans* worms should come from the same batch, so that the worms studied have approximately the same age. To start the experiments, 8 to 10 L4 (young adult) worms are recommended. The two groups of worms should also be fed on the same batch OP50 bacterial lawn, so that the *E. coli* bacteria the worms eat are as similar as possible. The only exception is that the MNP group of worms should have their lawn supplemented with a small volume of rhodamine-tagged $CoFe_2O_4$ MNPs. The analysis of the worms with the confocal microscope should occur on the same day, so that the ages of the worms in the images to be analyzed are the same.

The analysis of the *C. elegans* worms with fluorescing neurons and MNPs should be completed carefully to avoid the problems of bleed over and autofluorescence. To minimize the autofluorescence effects, the control group of worms should be analyzed first on the confocal microscope. Initially only the rhodamine channel (stimulation by the 543 nm laser) should be used; the gain of the image should be adjusted until any autofluorescence disappears. Then the green channel (488 nm laser) can be opened and the gain adjusted so an image can be captured. After the analysis of the control worms, the study of the worms fed MNPs can begin being careful to maintain the level of gain in the red channel at the low level determined in the control worm analysis. By keeping the gain at this low level, the effects of autofluorescence should be minimized. The mutant worms fed rhodamine-tagged MNPs should be analyzed in the same manner as the control worms: red channel first, then with both. The longer the worms are exposed to the light from the green channel, the higher the risk for bleed over to occur. This will cause fluorescence to occur in the red channel that does not correspond to the rhodamine-tagged MNPs. By following the procedure outlined above, the effects of bleed over and autofluorescence on the images collected should be minimized.

To quantitatively determine if any rhodamine-tagged $CoFe_2O_4$ MNPs are localizing to the neurons of the mutant worms, ImageJ can be used to measure the areas of fluorescence in images collected from the confocal microscope. By analyzing the overlap of red fluorescence in areas of green fluorescence, a percent of neural areas that contain MNPs can be calculated. These data would help determine if the MNPs are capable of moving throughout the body of the worm. If it is possible for the MNPs to move into the nervous systems of the worms, it may be possible through surface modifications to control the localization behavior of magnetic nanoparticles in these organisms.